



Hydrological influence on the evolution of a subtropical mangrove ecosystem during the late Holocene from Babitonga Bay, Brazil

Allana Queiroz de Azevedo ^{a,b,*}, Francisco J. Jiménez-Espejo ^{c,d}, Marlon Carlos França ^{b,e}, Antonio García-Alix ^f, Fernando A. Borges da Silva ^b, Luiz C.R. Pessenda ^g, Marcelo C.L. Cohen ^b, Neuza A. Fontes ^b, Vanessa C. Pinheiro ^b, Kita Macario ^h, João C.F. Melo Jr ⁱ, Marisa de C. Piccolo ^g, José A. Bendassolli ^g

^a Programa de Pós-Graduação em Geoquímica, Universidade Federal Fluminense, Niterói 24020-141, Rio de Janeiro, Brazil

^b Graduate Program of Geology and Geochemistry, Federal University of Pará, Institute of Geosciences, Belém 66075-110, Pará, Brazil

^c Instituto Andaluz de Ciencias de la Tierra, Consejo Superior de Investigaciones Científicas, Armilla 18100, Spain

^d Research Institute for Marine Resources Utilization (Biogeochemistry Program), JAMSTEC, Yokosuka, Kanagawa 237-0061, Japan

^e Oceanography and Climate Laboratory, Federal Institute of Education, Science and Technology of Espírito Santo, Piúma 29075-910, Espírito Santo, Brazil

^f Departamento de Estratigrafía y Paleontología, Facultad de Ciencias, Universidad de Granada, Granada 18071, Spain

^g University of São Paulo, CENA, Piracicaba 13416-000, São Paulo, Brazil

^h Radiocarbon Laboratory (LAC-UFF), Universidade Federal Fluminense, Physics Department, Niterói 24210-346, Rio de Janeiro, Brazil

ⁱ Anatomy and Vegetal Ecology Laboratory, University of Joinville, Joinville 89219-710, Santa Catarina, Brazil

ARTICLE INFO

Editor: Howard Falcon-Lang

Keywords:

Mangrove

South America

Precipitation

Pollen grain

Intertropical Convergence Zone

ABSTRACT

Mangroves are key ecosystems which respond to global changes in tropical and subtropical regions worldwide. We describe late Holocene mangroves that established close to the southernmost limit (28°S) for this type of ecosystem in South America. Our findings are based on a ^{14}C dated core obtained from Babitonga Bay, Santa Catarina State, Brazil ($26^{\circ}12'\text{S}$, $48^{\circ}33'\text{W}$). Analysis of palynology, sedimentary facies, isotopic and elemental data shows that mangrove establishment took place ~ 500 yrs. B.C.E., following an increase in humidity, and expanded further during the Roman Warm Period and at the end of Dark Age Cold Period. Mangrove and precipitation proxies records appear to be sensitive to rainfall patterns imposed both by the expansion/retraction of the Intertropical Convergence Zone and also the interaction with the South Atlantic Subtropical Anticyclone which affects coastal region due to sea surface temperature variations.

1. Introduction

The mangrove ecosystem performs several natural functions of great climatological and economic importance. It is present along tropical and subtropical coastlines (Baran, 1999; de Rodrigues et al., 1999; Barbier, 2000; Nagelkerken et al., 2008; Cannicci et al., 2008) and protects these areas due to its aerial roots that trap sediments, stabilizing the substrate of intertidal areas, and thereby reducing erosion (Thampanya et al., 2006). In addition, roots, trunks, and canopy dissipates storm surges (McIvor et al., 2012a) and waves (McIvor et al., 2012b).

Previous studies have shown that mangroves can reduce up to 66% of wave energy in the first 100 m of forest width (McIvor et al., 2012b; McIvor et al., 2016), and these forests can provide adaptive defenses,

accompanying the rise in sea level through vertical accumulation (McKee, 2011; Krauss et al., 2014). This means significant annual flood protection for people and property both from cyclones and the more regular (non-cyclonic) high wave and swell events, hence savings of over \$65 billion per year for the United States, for instance, in terms of flood protection benefits (Menéndez et al., 2020).

Besides, these ecosystems can store vast amounts of carbon. The fact that they are among the most carbon-rich forests in the tropics (Donato et al., 2011) lends them added value in the global warming trend and future scenario. Yet, the loss of mangrove ecosystems could be greatly intensified if sea-level rise and drought are enhanced in coastal areas, as forecast for the future (IPCC, 2013). The study of past environmental changes serve to improve our understanding of future climate scenarios

* Corresponding author at: Programa de Pós-Graduação em Geoquímica, Universidade Federal Fluminense, Niterói 24020-141, Rio de Janeiro, Brazil.

E-mail addresses: allanaazevedo@id.uff.br (A.Q. Azevedo), fjjspejo@ugr.es (F.J. Jiménez-Espejo), agalix@ugr.es (A. García-Alix), pessenda@cena.usp.br (L.C.R. Pessenda), kitamacario@id.uff.br (K. Macario), mpiccolo@cena.usp.br (M.C. Piccolo), jab@cena.usp.br (J.A. Bendassolli).

by providing information on when mangrove environments were established or how they reacted to millennial-to-centennial variations in climate during the Holocene (Jones et al., 2019).

Mangrove expansion worldwide has been limited due to changes in precipitation, salinity, tide level, topography (Schaeffer-Novelli et al., 1990; Kathiresan and Bingham, 2001; Schaeffer-Novelli et al., 2016) sea-level rise, changing ocean currents, and increased storminess (Duke et al., 1998; Ellison, 2002; Spalding et al., 2010; McKee et al., 2012). In Brazil, mangroves occur from Cabo Orange (5° N) to Laguna (Santa Catarina State), the southernmost limit for South American mangroves (Lat. 28° S) (Cintrón-Molero and Schaeffer-Novelli, 1992), covering an area of approximately 14 thousand km 2 (Schwamborn and Saint-Paul, 1996). Globally mangroves have declined over the past decades, from $\sim 140,000$ km 2 in 2000 to $\sim 132,000$ km 2 in 2014 (Hamilton and Casey, 2016).

At this region studies are mainly focused on increasing air temperature due paleoclimatic changes and sea level rise as the drivers of mangrove forests expansion (Behling, 1995; França et al., 2019; Cohen

et al., 2020). Comparison between palynological and precipitation records are scarce. Here we address this issue comparing two cores on margins of Babitonga Bay (Southern Brazil, Lat. 26° S), close to the southernmost limit (28° S) for mangroves ecosystem growth in South America, with records sensitive to the South American monsoon system (e.g., Botuverá Cave, Bernal et al., 2016).

Thus, this study was carried out by sedimentary facies, palynology, isotopes ($\delta^{13}\text{C}$), and elemental data (C:N ratio) dated by radiocarbon analysis with three main goals: (1) to ascertain when the mangroves of Babitonga Bay were established; (2) to propose a paleoenvironmental reconstruction of the study area; and (3) to determine the main forces driving the mangrove development.

2. Study site

Our study site is located at margins of Babitonga Bay, northeastern of Santa Catarina State, Southern Brazil (Fig. 1a). At its northeastern bank we collected a shallow core measuring 200-cm-long (present study, SF8:

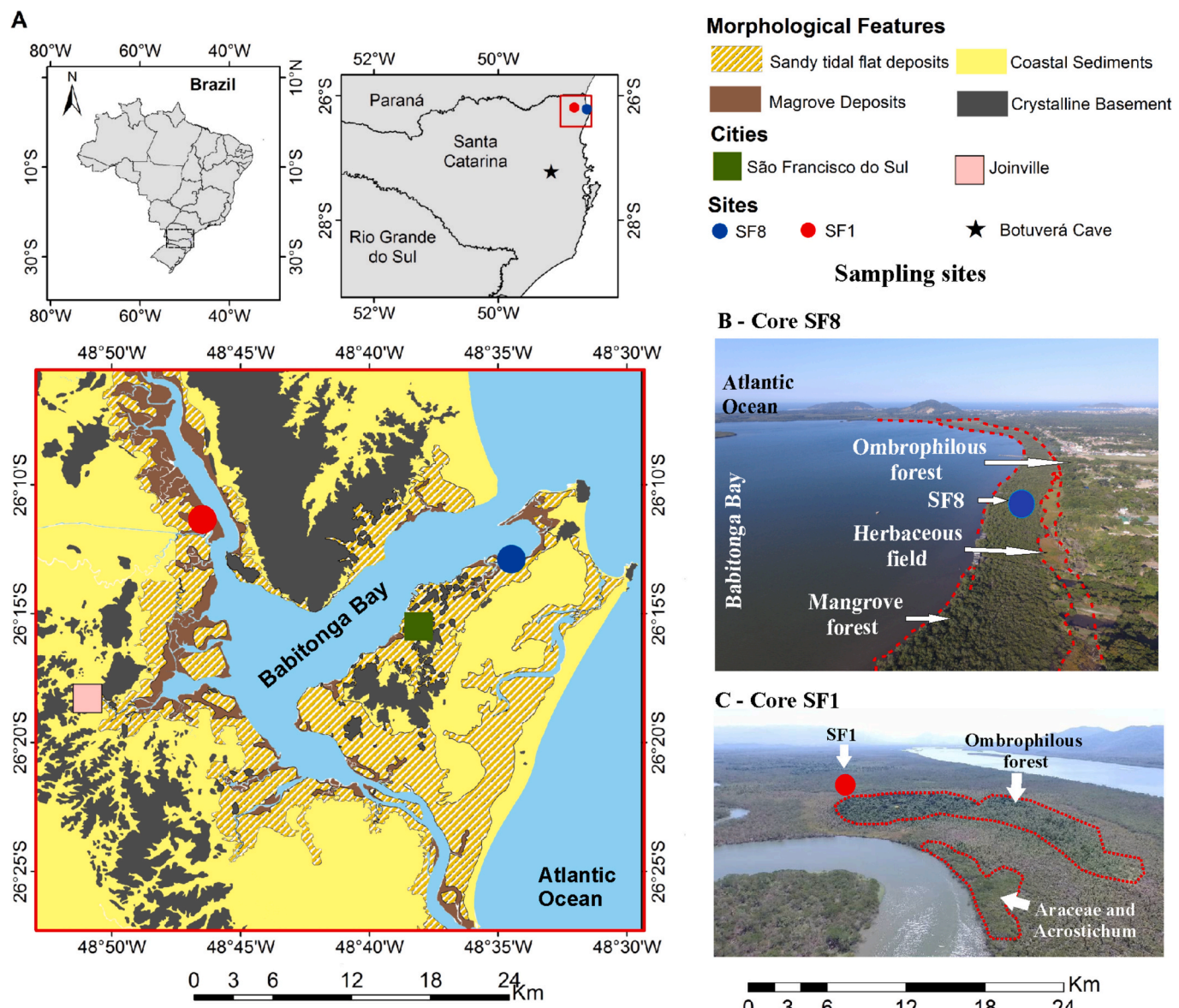


Fig. 1. Localization of discussed sites: A) core SF8 (this study), core SF1 (França et al., 2019) and Botuverá Cave (Bernal et al., 2016) in Santa Catarina State, southern Brazil; B) Surrounding modern vegetation of SF8 sampling site delimited by red dashed lines and C) Panoramic view of Babitonga Bay and vegetation type around SF1 sampling area. Map of Babitonga Bay were made with shapefiles available on Geodiversidade do Estado de Santa Catarina Project of Geological Survey of Brazil (Viero and Silva, 2016). (For interpretation of the references to colour in this figure legend, the reader is referred to the web version of this article.)

26°12'S/ 48°33'W). The core SF1 (França et al., 2019), further approached, is 300-cm-long and was recovered from northwestern margin (Fig. 1b, c). The former core is located 120 km far from Botuverá Cave (27°13'S; 49°09'W, Bernal et al., 2016) and 6 km from the South Atlantic Ocean. Modern vegetation surrounding the bay comprises herbaceous field, mangrove and ombrophilous forests. Tidal flats of Babitonga Bay are expressively marked by mangroves, representing ~75% of the mangroves in Santa Catarina State (Herz, 1991).

Babitonga Bay is under influence of rivers, tides, and waves (Mazzer and Gonçalves, 2012). Riverine input into Babitonga Bay results from Cachoeira, Palmital, Cubatão, and Parati hydrographic basins (Barros et al., 2010). Warm (> 20 °C) and saline (> 36.2) Tropical Water (Stramma and England, 1999) from the South Atlantic Ocean overruns this bay once a day as a semidiurnal tide (FEMAR, 2000). Mean tidal range is ~0.84 m, while the maximum high tide is ~1.9 m (DHN, 2017), thus characterizing a micro-tidal coast.

This region has a humid mesothermal climate with a hot summer and no dry season (Köppen classification). Moisture content is 68% to 89%, the monthly average temperature ranges from 16.5 to 25.6 °C, and the monthly rainfall ranges from 402 mm (January) to 106 mm (August) (Gonçalves et al., 2006). Rainfall and temperature are highest in January and March (summer), and decrease from June to August (winter) (FUNDEMA, 1994).

The precipitation at our study site is influenced by two major components of atmospheric dynamics within South Atlantic Monsoon System (SAMS) scope: South Atlantic Convergence Zone (SACZ) and South Atlantic Subtropical Anticyclone (SASA), both associated to South

Atlantic surface temperature (Liebmann and Mechoso, 2011). During the austral summer, positives South Atlantic surface temperature anomalies boosts the Intertropical Convergence Zone (ITCZ), promoting its expansion and migration to more southward position. From that low-level winds flow westward, transporting moisture into the Amazon basin. However, it is blocked by the Andes ridge and shift its direction to the southeast/southern region forming a ‘wind corridor’ called South Atlantic Low-Level Jet (SALLJ) (Garreaud et al., 2009; Marengo et al., 2012; Vuille et al., 2012; Zhou and Lau, 1998). Near middle latitudes, SALLJ and the low-level moisture convergence favors deep convection, forming the SACZ rain belt (Kodama, 1992) (Fig. 2). The second component, SASA, is closely related to sea surface temperature (SST) mode of South Atlantic Subtropical Dipole (SASD). SASD, dominant mode of coupled ocean-atmosphere (Venegas et al., 1997), has a dipole structure oriented in the northeast-southwest direction (Haarsma et al., 2005; Morioka et al., 2011; Nnamchi et al., 2011). SASD positive (negative) phase is related to negative (positive) SST anomalies at northeastern pole (0° and ~30°S) and positive (negative) SST anomalies at southwestern pole (~30°S and 50°S) (Morioka et al., 2011). This positive phase is related to intensified evaporation in the Southwestern Pole and, consequently, increased moisture advection to SE and Southern Brazil by the SASA, resulting in wetter conditions in this region. The reverse situation creates the negative phase of SASD (Wainer et al., 2014).

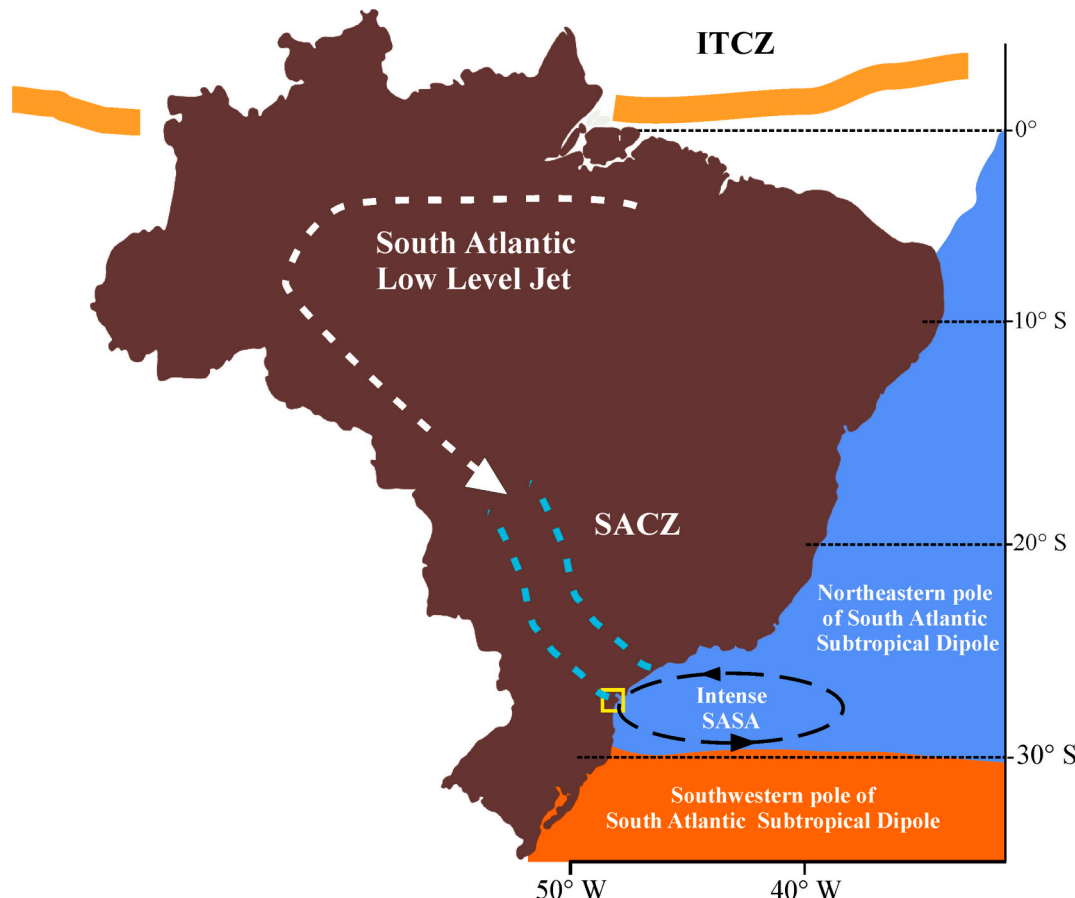


Fig. 2. Main drivers of Babitonga Bay hydrology: 1) Intertropical Convergence Zone (ITCZ) expansion feeds the South Atlantic Low-Level Jet (SALLJ), bringing moisture to rain belt South Atlantic Convergence Zone (SACZ) and, 2) Positive phase of South Atlantic Subtropical Dipole (warmer waters (orange colour) at southwestern pole and colder waters at northeastern pole), which provides less evaporation and moisture advection at northeastern pole by South Atlantic Subtropical Anticyclone (SASA). Yellow square represents study area site. (For interpretation of the references to colour in this figure legend, the reader is referred to the web version of this article.)

2.1. Geologic and geomorphological settings

The study area is inserted within the Joinville geologic map (SG.22-Z-B) (Fig. 3a). It comprises four geologic units: a crystalline basement (Luis Alves Microplate and Paranaguá Domain), diabase dikes (Serra Geral Formation), and Cenozoic unconsolidated sediments (recent deposits). The geologic-geotectonical structure of this area is a result of the independent development of four amalgamated geotectonic blocks in Neoproterozoic times, during the formation of the Gondwana Supercontinent. The Luis Alves Microplate geotectonic block is the largest unit (Basei et al., 1992). These rocks were later covered by Paleozoic to Mesozoic sedimentary rocks, by Cretaceous volcanic rocks of Paraná basin, and by Holocene unconsolidated sediments.

The origin of all estuarine complexes on the eastern Brazilian coast is strongly related to Quaternary sea-level oscillations (Villwock et al., 1986; Tomazelli and Villwock, 2000). After the mid-Holocene sea-level highstand, at about 5100 cal. Yrs. BP (Angulo and Lessa, 1997; Angulo et al., 1999; Lessa et al., 2000; Martin et al., 2003), coastal river valleys and coastal plains were flooded, this was followed by a relative sea-level fall until reaching the current mean sea-level, conforming the current landscape. The study site is divided into the following geomorphological sub-units: Babitonga upper estuary, lower littoral, alluvial and marine plain, hills and residual elevations, Serra do Mar and plateau (Fig. 3b)

(Gonçalves and Kaul, 2002; Rosa, 2002; IBGE, 2004; Vieira and Horn Filho, 2007).

3. Material and methods

3.1. Fieldwork and sampling

The fieldwork was carried out in September 20–30, 2016, at the northeastern margin of Babitonga Bay, northeastern coast of Santa Catarina, where we collected the core SF8 ($26^{\circ}12'S$, $48^{\circ}33'W$) with a Russian sampler. After recovering, it was properly wrapped (with a tube and a PVC plastic), and kept under 4°C temperatures refrigeration to preserve organic matter.

3.2. Sedimentary facies analysis

Description of sediments core SF8 was based on Walker and James's (1992) model that proposes the following descriptive and interpretative criteria such: 1) facies individualization, which takes into account the geometry of bedding, sedimentary structures, textures, lithological composition, fossiliferous content, and 2) facies association and depositional model. The core coloring was described based on Munsell's colour chart (Munsell Colour, 2009).

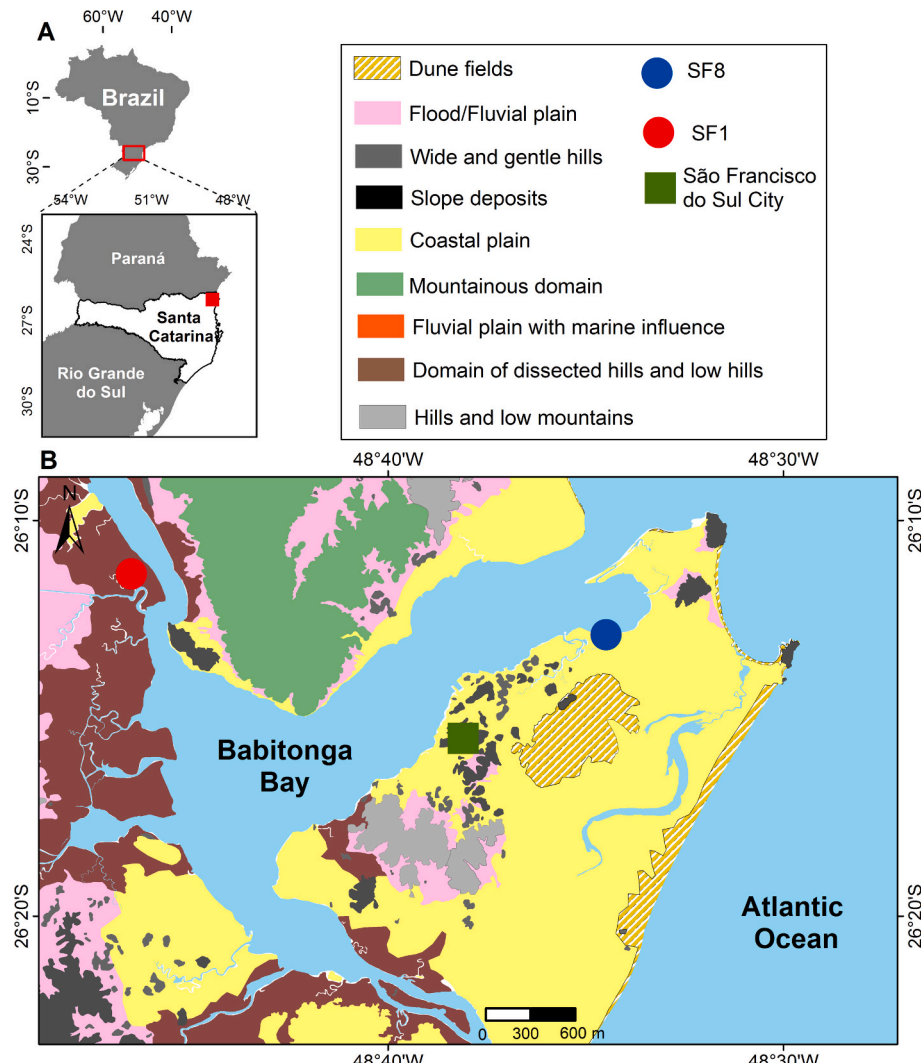


Fig. 3. A) Delimitation of Joinville geologic map (SG.22-Z-B) (red square), which both cores SF8 and SF1 are inserted, and B) Geomorphologic map of study site. Shapes are available on Geodiversidade do Estado de Santa Catarina Project of Geological Survey of Brazil (Viero and Silva, 2016). (For interpretation of the references to colour in this figure legend, the reader is referred to the web version of this article.)

3.3. Granulometric analysis

Sampling for granulometric analysis were carried out every five centimeters, totaling forty-one samples throughout the entire core. Before particle size reading all samples were chemically treated with hydrogen peroxide (10%) to remove organic matter and placed into ultrasound to disperse sedimentary particles. Granulometric reading was performed with a Laser Particle Size SHIMADZU SALD 3101 and grain sizes were displayed according to Wentworth's distribution (Wentworth, 1922).

3.4. Palynological analysis

3.4.1. Clearing procedure

A total of 1 cm³ was sampled from each interval of 5 cm to be chemically cleaned following Colinvaux et al. (1999) protocol. At first step, we add tablets of exotic marker Lycopodium (Stockmarr, 1971) and 10 ml of 10% Hydrochloric Acid (HCl) in all forty-one samples to remove carbonate (CO₃)⁻² of both matrix of samples and Lycopodium. After each acid (10 ml) input step, we performed repeatedly the mixing, centrifugation, and distilled water addition in order to remove the applied acid. Second step involved the usage of Hydrofluoric Acid (HF) to remove the silica (SiO₂). We left samples with this acid for 24 h and then we removed it. Third step consisted on adding glacial acetic acid (C₂H₄O₂) to dehydrate samples and avoid dangerous reactions at the final step, acetolysis (H₂SO₄ and C₄H₆O₃). During acetolysis we removed cellulose and polysaccharides, which often mask the internal structures of pollen grains and make harder the correct taxonomic identification.

3.4.2. Pollen taxonomy and cluster analysis

Taxonomic identification of SF8 pollen grains was accomplished mainly up to the hierarchical family level based on morphological descriptions of quaternary palynology published by Roubik and Moreno (1991), Behling (1993), Colinvaux et al. (1999), Neves et al. (2001), and Bauermann (2003). Besides, we also consulted the Neotoma Paleoecology database, as well as the pollen database from Laboratory C-14 of the Center for Nuclear Energy in Agriculture of the University of São Paulo (CENA-USP).

Cluster analysis was performed by CONISS, which is a Fortran programming language for stratigraphically constrained cluster analysis applied on palynological data by the incremental sum of squares method (Grimm, 1987) by means of Tilia software (Version 1.7.16) (Grimm, 1990). The criteria used to define the heights of nodes connecting clusters in generated dendograms by this method includes: enhance in dispersion at each stage (Gordon, 1981), total dispersion at each stage (Ward, 1963; Anderberg, 1973), within-cluster dispersion of individual clusters (Pielou, 1984), and mean within-cluster dispersion of individual clusters (Orloci, 1967; Birks et al., 1975).

3.5. Radiocarbon dates and age model

The chronology of core SF8 was obtained through four radiocarbon dating on samples SF8-60_65, SF8-115_120, SF-170_175, and SF-190_195. Each sample comprised 10 g of bulk organic matter, where shells, seeds, and roots were mechanically removed to avoid contamination. These samples were treated with 2% HCl to remove carbonate, rinsed several times with distilled water, and dehydrated in an oven at 40 °C. This initial treatment was performed at Laboratory C-14 of the Center for Nuclear Energy in Agriculture of the University of São Paulo (CENA-USP). The graphitization process was performed at the Radio-carbon Laboratory of the Fluminense Federal University (LACUFF) on samples SF8-60_65 and SF8-115_120. These pretreated samples were dated by Accelerator Mass Spectrometry (AMS) at the Center for Applied Isotope Studies (CAIS, University of Georgia, USA) and the residue of samples SF-170_175, and SF-190_195 was submitted to BETA Analytic (Miami, USA) for AMS analysis.

The complete age-depth model (Fig. 4) was built with Bacon v. 2.2 package, which uses Bayesian statistics to reconstruct Bayesian accumulation histories for sedimentary deposits within the R software (Blaauw and Christeny, 2011). The ¹⁴C ages were normalized to δ¹³C value of -25‰ VPDB and calibrated using SHCal20 calibration curve (Hogg et al., 2020) on CALIB 8.2 software (Stuiver et al., 2021) (Table 1). Results were displayed as calibrated years before present (cal yr B.P.) at age model and as Before Common Era (B.C.E.)/Common Era (C.E.) to make easier the comparison of exploited dataset.

3.6. Isotopic and elemental data

The sampling to isotopic and elemental data of core SF8 followed the same reasoning of 5 cm intervals, but to each depth we collected ~35 mg, thus we gathered a total of 82 samples (41 to former analysis and 41 to later). These samples were chemically treated with 5% Hydrochloric Acid (HCl) to remove carbonate, washed with distilled water, dried at 50 °C, and homogenized. δ¹³C analysis were performed by ANCA SL2020 mass spectrometer at the Stable Isotope Laboratory (at CENA/USP). Total organic carbon (TOC) and total nitrogen (TN) were read on LECO Truspec CHNS elemental analyzer at the Laboratory of Nutrient Cycling (at CENA/USP). The δ¹³C results are expressed in ‰ with reference to VPDB (Vienna Pee Dee Belemnite) and ± 0.2‰ of analytical precision (Pessenda et al., 2004). TOC and TN results are expressed as a percentage of dry weight, with analytical precisions of 0.09% (TOC) and 0.07% (TN).

4. Results

4.1. Sedimentation ages and rates

The ¹⁴C data of core SF8 represents a sedimentary record covering ~5 kyr B.P. Dated depths of core SF8 revealed the following ages displayed in cal yr B.P. (1σ): 190–195 cm (4727 ± 35), 170–175 cm (3706 ± 22), 115–120 cm (1345 ± 23), and 60–65 cm (591 ± 24), showed in years C.E. on Table 1. These results showed respective sedimentation ages (exhibited here as mm/yr) from deepest to shallowest depth: 0.41, 0.46, 0.87, and 1.06. Beyond radiocarbon dating of core SF8 we also used core SF1 ¹⁴C ages to compare mangrove and spores content behavior of both records.

4.2. Facies association and pollen content

The sedimentary analysis of core SF8 allowed the identification of six facies and the grouping into three facies associations (FA), from oldest to youngest: FA1, FA2, and FA3 (Table 2, Fig. 4). Two fining-upward cycles were identified, the first from 200 cm to 100 cm and the second from 100 cm to the surface.

Trees and shrubs as *Alnus*, Annonaceae, Bignoniaceae, Meliaceae, *Brysonima*, Burseraceae, Cannabaceae, Celastraceae, Icacinaceae, Malpighiaceae, Mimosoideae, Proteaceae, *Smilax*, Sapotaceae, Phyllanthaceae, Sapindaceae, and Simlocaceae showed the lowest values (<3%) throughout all facies association and for that reason were excluded from pollen diagrams. The same was applied to herbs with <2% values as Apiaceae, Begoniaceae, *Borismene*, Malvaceae, and Ranunculaceae.

4.2.1. Facies association 1 (FA1)

Sedimentary deposits of FA1 represents the base of core SF8 and comprises depth 200 to 150 cm. It is composed by sand (18–100%) with clay levels (0–64%), and silt (0–18%) divided into tabular and laterally continuous layers of sands with plane-parallel (facies Pp, 30 cm thick) and cross-bedding sand (facies Cb, 20 cm thick) (Fig. 4). These facies vary from coarse to medium-grained sand, brownish-yellow in colour, and disjointed valves of bivalve mollusks represents their macrofossiliferous contents. FA1 contact with FA2 is transitional and marked by fine sand and mud laminations.

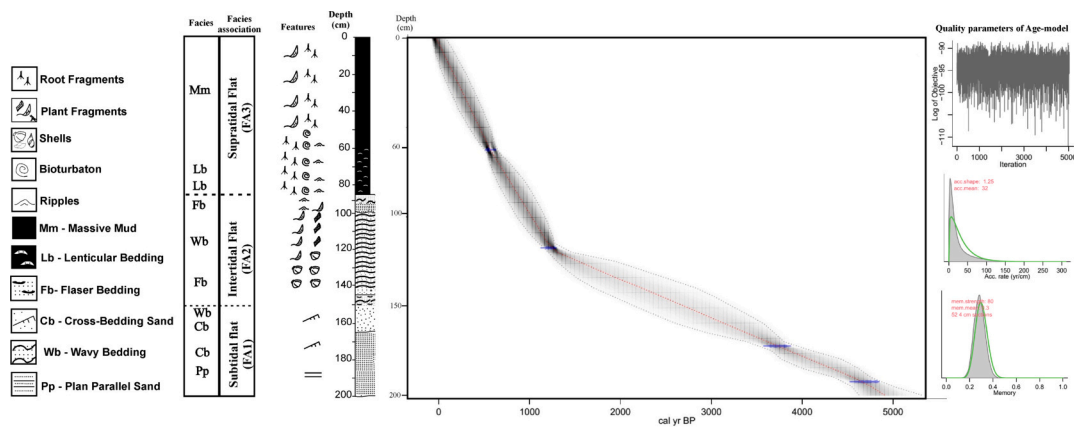


Fig. 4. Lithostratigraphic profile of 200-cm-long core SF8 displaying facies, features, labels, facies association, Bayesian age model and quality parameters of age modelling.

Table 1

Sediment samples selected for radiocarbon dating and results with, laboratory code-number, interval depth (m), material type, radiocarbon ages (cal yr B.P., 1σ and 2σ), common era (C.E.) ages and median of calibrated ages displayed in C.E. Age calibration has been performed by means of the SHCal20 calibration curve (Hogg et al., 2020) and CALIB 8.2 software (Stuiver et al., 2021).

Core	Laboratory Code-Number	Depth (m)	Material	Ages (^{14}C yr BP, 1σ)	Ages (cal. yr BP, 2σ)	Common Era (yr C.E.)	Median Probability (yr C.E.)	Reference
SF8	UGAMS-28,837	0.60–0.65	Bulk sed.	591 ± 24	626–518	1324–1432	1404	This study
SF8	UGAMS-28,838	1.15–1.20	Bulk sed.	1345 ± 23	1279–1178	671–772	724	This study
SF8	Beta - 585,259	1.70–1.75	Bulk sed.	3490 ± 30	3835 – 3629	(–1886) – (–1680)	-1774	This study
SF8	Beta - 585,260	1.90–1.95	Bulk sed.	4210 ± 30	4835–4579	(–2886) – (–2630)	-2764	This study
SF1	UGAMS-28368	0.75–0.80	Bulk sed.	1070 ± 20	960–916	990–1034	1006	França et al., 2019
SF1	UGAMS-28372	1.10–1.15	Bulk sed.	950 ± 20	904–739	1046–1211	1132	França et al., 2019
SF1	UGAMS-28848	1.60–1.65	Bulk sed.	1570 ± 20	1512–1353	438–597	548	França et al., 2019
SF1	UGAMS-31233	2.30–2.35	Bulk sed.	1870 ± 30	1862–1636	88–314	182	França et al., 2019

Pollen diagrams (Figs. 5, 6 and 7) display the data by each depth. Our dataset description involves the total sum of vegetation type (e.g., \sum herbs, \sum palms) of all depths that compose each facies association. Thereby, paleo-palynological records of FA1 (\sum pollen grain = 816) are composed by herbs, (33.33%, \sum = 272), trees-shrubs (29.04%, \sum = 237), spores (24.02%, \sum = 196), and palms (13.60%, \sum = 111). Poaceae (5–67%) and Asteraceae (1–11%) are the main representative family of herbs. As major trees and shrubs we found *Alchornea* (4–12%), Fabaceae (2–9%), *Hedyosmum* (1–10%), and *Ilex* (1–11%). Arecaceae (2–18%) is the only family that characterizes palms in all facies association. Spores are evidenced by Polypodiaceae (3–24%) and trilete spores (1–19%). Typical mangrove pollen grains assemblage (*Avicennia*, *Laguncularia*, and *Rhizophora*) were not observed.

4.2.2. Facies association 2 (FA2)

The central portion of core SF8 is depicted by facies association 2 (FA2) that ranges between 150 and 85 cm. It is composed by sand layers (15–100%) that intercalates between silt (0–65%) and clay (0–18%) through alternation of tabular and laterally continuous layers of heterolithic facies as flaser bedding (Fb) and wavy bedding (Wb). Coloring of these deposits fluctuate from brownish-yellow (150 to 142 cm), very dark greenish gray (142 to 100 cm), and dark greenish gray (100 to 85 cm). Macrofossiliferous content includes plant/trunk fragments and expressive quantitative bivalve mollusk shells. The contact of FA2 with FA3 is transitional and marked by the presence of fine sand and small mud lenses.

We observe a higher palynological content (\sum = 2333), than previous one. Outstanding in this association is the beginning of mangroves

with development of *Laguncularia* (1–20%) and *Avicennia* (1–2%). Throughout FA2 *Laguncularia* is continuous, whereas *Avicennia* are discontinuous and represented by lower values. Vegetation type such as herbs, trees-shrubs, and palm trees reach its maximum values (Fig. 5). Herbs are mostly represented by Poaceae (12–77%), Cyperaceae (1–6%), and Asteraceae (2–11%). *Alchornea* (1–57%), Fabaceae (2–19%), *Hedyosmum* (2–11%), Rubiaceae (2–11%), Melastomataceae/ Combretaceae (1–8%), Myrsinaceae (1–8%), and *Ilex* (1–7%) are the predominant trees and shrubs (Fig. 6). The Arecaceae family ranged from 10 to 45%. Spores are characterized by Polypodiaceae (6–55%) and trilete spores (6–26%) (Fig. 7).

4.2.3. Facies association 3 (FA3)

Sedimentary deposits from 85 cm to surface displays tabular and laterally continuous layers of clay (0–64%) along with silt (0–18%) containing sand lenses (20–60%), which are expressed by lenticular bedding (Lb) and massive mud (Mm) facies, grouped into FA3. Its major macrofossiliferous content are roots and plant fragments. In colour, it ranges from very dark greenish gray (85–50 cm) and very dark brown (50 cm to surface).

The mangrove forest (\sum = 98) is composed by *Laguncularia* (2–8%) and *Avicennia* (1–2%), and *Rhizophora* (1–10%). Comparatively to FA2, we observed a decreasing of trees and shrubs (\sum = 590), herbs (\sum = 530), palm trees (\sum = 169), and spores (\sum = 348). The former vegetation type is mainly represented by *Alchornea* (2–29%), Melastomataceae/ Combretaceae (1–12%), *Podocarpus* (1–10%), Moraceae (1–9%), Myrsinaceae (1–7%), and Myrtaceae (1–7%). Similarly, herbs content diminished and was represented predominantly by Poaceae

Table 2

SF8 facies, description and sedimentary process of each facies association from the base to top: subtidal flat (Facies Association 1, FA1), intertidal flat (Facies Association 2, FA2) and supratidal flat (Facies Association 3, FA3).

Facies	Description	Sedimentary Process	FA
Massive Mud (Mm)	60 cm thickness deposits of mud deposit very dark brown coloring with leaves and roots fragment	Deposition from suspension under low energy conditions	Supratidal Flat (FA 3)
Lenticular Bedding (Lb)	15 cm thickness deposits of sand and clay very greenish gray coloring dark with bioturbation and root fragments	Alternation between suspension and traction processes	
Wavy Bedding (Wb)	50 cm thickness deposits with clay and sand of yellowish-brown coloring 6/8 with shell fragments roots, leaves and tree trunks	Alternation between suspension and traction processes	Intertidal Flat (FA2)
Flaser Bedding (Fb)	15 cm thickness deposits with sand and clay dark greenish gray coloring with leaves fragments	Alternation between suspension and traction processes	
Cross-bedding Sand (Cb)	Medium-grained sand with ripples / cross stratification and 20 cm thickness deposit.	2D bedforms migration under unidirectional flow and lower flow rate	Subtidal Flat (FA1)
Sands with plan-parallel cross-bedding (Pp)	Medium to fine sand with plan-parallel cross-bedding and 30 cm thickness deposit.	Sandy Sheet Migration under unidirectional flow and lower flow rate	

(4–44%), Asteraceae (1–14%), and Cyperaceae (1–8%). Polypodiaceae (6–55%) and trilete spores (1–26%) comprised the content of spores.

4.3. Cluster analysis – CONISS

Palynological cluster analysis performed through CONISS provided three main groups (stratigraphic zones), which present similarities regarding pollen grains amount of constrained adjacency (depths). These zones agree and reinforces the three facies association previously identified during the fieldwork (subtidal, intertidal and supratidal flat) (Fig. 6).

4.4. Elemental and isotopic analysis

Elemental data regarding the stratigraphic profile reveal a topward increase in total organic carbon (TOC), as well as increases in total nitrogen (TN) and in the C:N ratio. Our TOC and TN data showed a strong positive correlation coefficient ($r^2 > 0.9$). The TOC and TN results are between 0.33% and 17.39% ($\bar{X} = 6.43\%$) and 0.07–0.61% ($\bar{X} = 0.26\%$),

respectively. The C:N values varied from 4.33 to 32.61 ($\bar{X} = 18.44\%$). According to the stratigraphic profile, the C:N ratio behavior gradually increased topward, with a relation between TOC and grain size, and mangrove colonization (Fig. 5). The $\delta^{13}\text{C}$ values exhibit a relatively stable result from -27.47 to -22.43‰ ($\bar{X} = -24.64\text{‰}$). The $\delta^{13}\text{C}$ behavior revealed depleted isotopic values throughout the stratigraphic profile.

5. Discussions

Our pollen, sedimentary data, and elemental and isotopic results consistently suggest wetland development associated with the sedimentary evolution of a progradational tidalflat-succession (from sub to supratidal paleoenvironment) along the eastern margin of Babitonga Bay during the late Holocene. Here we assume the following late Holocene epochs: Roman Warm Period (RWP, 0 to 500 yrs. C.E.), Dark Ages Cold Period (DACP, 500 to 900 yrs. C.E.), Medieval Climate Anomaly (MCA, 900 to 1300 yrs. C.E.), and Little Ice Age (LIA, 1300 to 1850 yrs. C.E.) (Moreno et al., 2012) as there is no consensus about the precise

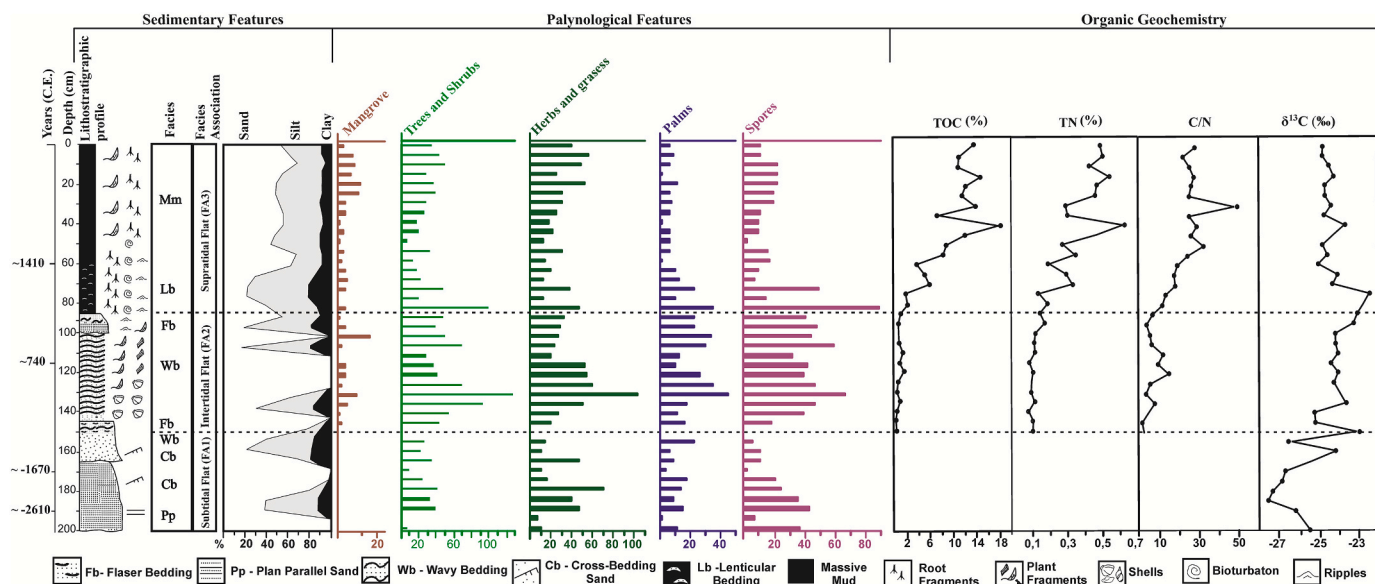


Fig. 5. Integrated data of sedimentary, palynological, radiocarbon dates (yrs C.E.) and geochemical features from core SF8. Total Organic Carbon (TOC), Total Nitrogen (TN), and C/N ratio from the base of core SF8 were not displayed due their low values.

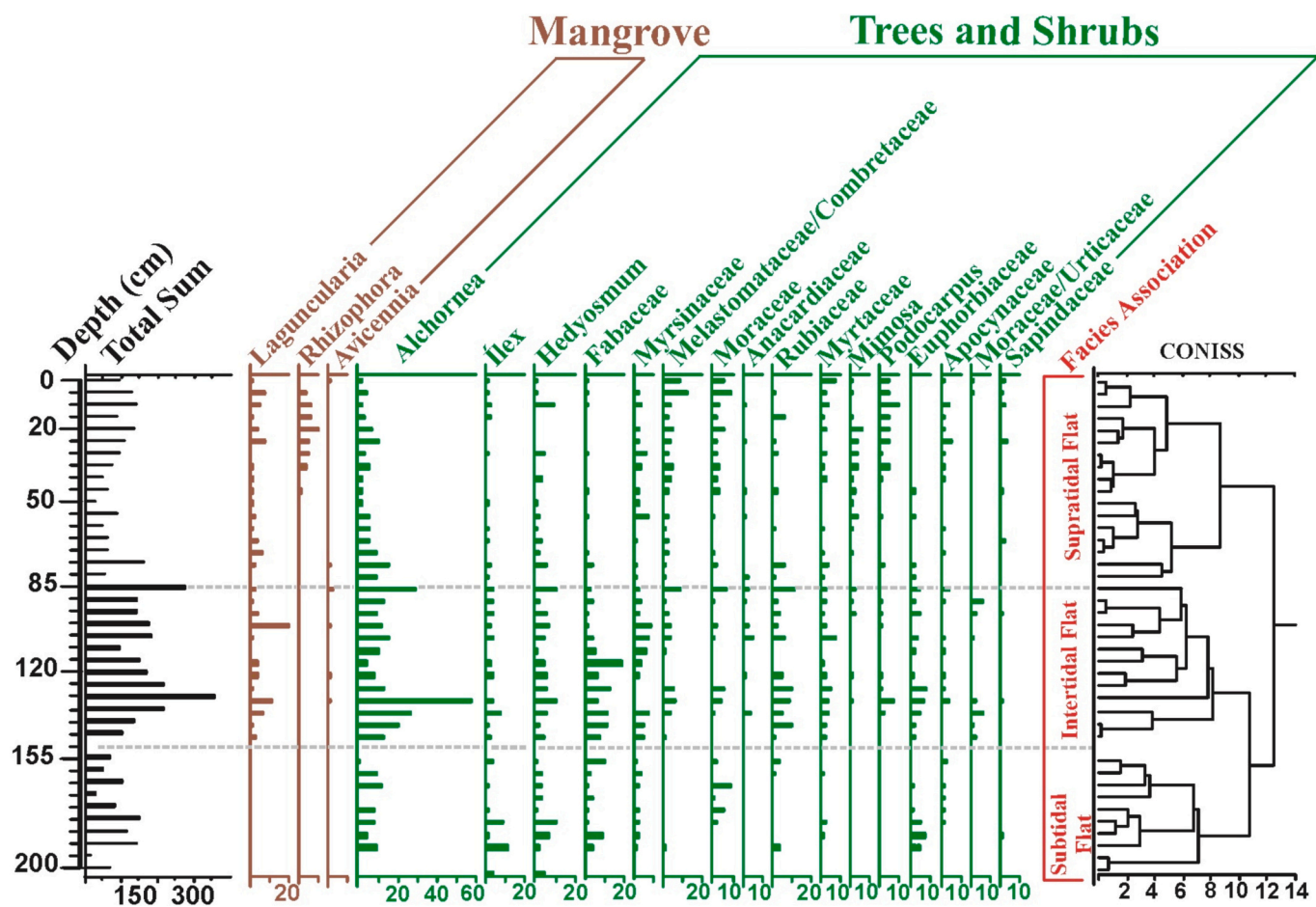


Fig. 6. Major genus of mangrove and trees/shrubs family from core SF8. Trees/shrubs that presented lower values (<3%) were not display.

temporal extent of these epochs (Neukom et al., 2019).

5.1. FA1 - Subtidal flat facies association (~2940 yrs. B.C.E. to ~750 yrs. B.C.E.)

The cross-bedding and plane-parallel cross-bedding sandy facies,

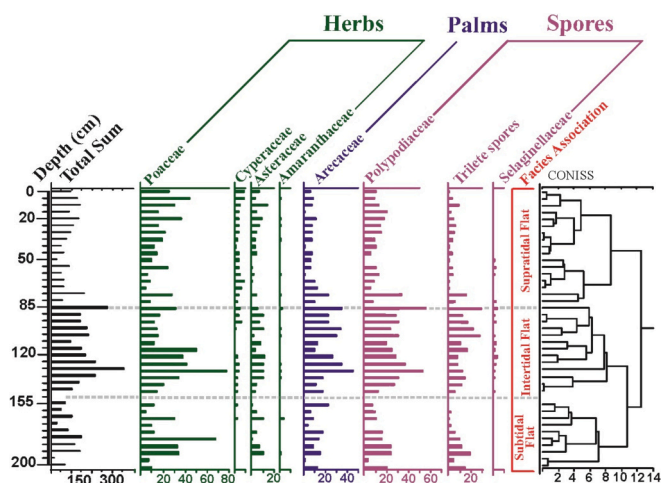


Fig. 7. Major herbs/grass, palms, and spores observed throughout core SF8. Herbs with lower values (<2%) were not displayed.

grouped into FA1, were interpreted as sand bars of a subtidal flat paleoenvironment formed between ~2940 to ~750 yrs. B.C.E. Its origin is tied to a migration of 2D bedforms and sandy sheets under unidirectional flow. Subtidal paleoenvironments with those sand bars is the result of a flood-filled channel during high tides on sheltered environments as estuaries and lagoons (Li et al., 1992; Dalrymple et al., 2003; Fan, 2011) reflecting to channel-filling deposits at the base of a tidal flat (Dalrymple, 1992). Tidal dominance over other processes (e.g., influence of waves) is most common in areas of a huge tidal range (Walker and James, 1992); our study site, however, has a microtidal pattern (DHN, 2017). A possible explanation for this occurrence would be limited wave action due to topographic sheltering (Walker and James, 1992). High concentrations of sands due this sedimentological setting unfavored the organic matter preservation and its mineralization process, which is corroborated by our TOC and TN data.

Throughout subtidal flat development spores, trees-shrubs and palms showed lower values comparatively to herbs. High percentages of Poaceae as seen in our records (Fig. 7) are often interpreted as an increased openness induced by dry and/or low humidity climatic conditions (Absy, 1979; Absy et al., 1991; van der Hammen and Absy, 1994; Hooghiemstra and van der Hammen, 1998). However, our isotopic data showed $\delta^{13}\text{C}$ ranging from -27.7 to -24.15‰. These values are compatible with C₃ plants (Meyers, 1994), meaning humidity further corroborated by tropical rain forest taxa (e.g., *Alchornea*, *Didymopanax*, Melastomataceae, Myrsinaceae, Arecaceae, Myrtaceae, and Moraceae/Urticaceae) (Behling, 1997). Thus, the high values of herbs, mainly represented by Poaceae in subtidal flat, cannot be interpreted as marking a dry period; its pollination strategies (wind-pollinated) determine the abundance of this taxa and allowing it to produce a huge amount of pollen as opposed to other taxa (Bush et al., 2002). For this reason, Poaceae is massively over-represented in the lowland tropical forests, and contributes to the disproportionately high percentage and low production of taxa that are insect-pollinated (Faegri, 1966). Regarding this palynological context we can infer that subtidal flat vegetation recorded alternation of moisture supply, varying from more to less humid.

Precipitation patterns reconstructed by $\delta^{18}\text{O}$ speleothems from Botuverá Cave show the influence of ITCZ on southern South America throughout the late Holocene (Bernal et al., 2016). From ~2940 to ~750 yrs. B.C.E. $\delta^{18}\text{O}$ Botuverá Cave recorded variable depleted isotopic signal, suggesting increasing precipitation trend. This pattern is in agreement with our palynological data, where trees, shrubs and palms percentage were slightly lower than those of herbs, probably moving from a less to more moisture supply during subtidal flat development due to ITCZ influence.

5.2. FA2 - Intertidal flat facies association (~750 yrs. B.C.E. to ~1100 yrs. C.E.)

The gradational spectrum of heterolithic bedding (flaser, wavy and lenticular bedding), grouped together into FA2, reveals alternation between suspension and traction processes from ~750 yrs. B.C.E. to 1100 yrs. C.E. (~RWP, DACP, and beginning of MCA), which were interpreted as intertidal flat paleoenvironment. The aforementioned facies may be produced by episodic flooding on alluvial plains, or weak storms in offshore environments, yet they occur mostly in tidal settings where the regular presence of slack tides favors mud deposition (Reineck and Singh, 1980; Dalrymple, 2010). Their development calls for factors including wave protection, high sediment supply, and sufficient accommodation space over the short term. The margins of estuarine channels, such as our study site, show high potential the deposit of neap-spring cyclic sequences, especially in mega-tidal estuaries where tidal bores may occur (Daidu et al., 2013).

Intertidal flat onset is marked by favorable conditions such as muddy substrate and wetter paleoclimate, allowing mangrove establishment (~500 yrs. B.C.E.) and two expansion phases at ~220 yrs. C.E. (~first half of RWP) and at ~930 yrs. C.E. (end of DACP) at SF8. Its colonization was associated with continuous presence of *Laguncularia* and a few *Avicennia*. Genus *Laguncularia* is often correlated with areas of sandy substrates, with less salinity (Schaeffer-Novelli et al., 2000), however, it can develop in mud substrate and is conditioned to early or middle succession stages of mangroves (Soares, 1999; Menghini, 2004; Kilca et al., 2010). Referred genus indicates higher precipitation combined with enhancing sediment input to the basin, additional spaces for mangrove establishment, therefore, became available (González et al., 2006) and probably also warming climate (França et al., 2019).

Mangrove forests recorded by core SF1 is younger than SF8, which only appeared after ~360 yrs. C.E. Despite their distance (~24 km) and age difference our core revealed a mangrove species succession similar to SF1. Initially occurred *Laguncularia* establishment, later *Avicennia*, and finally, *Rhizophora* trees (França et al., 2019). According these authors, this succession pattern is related to temperature increase during the late Holocene. Furthermore, when compare the palynological association with precipitation pattern recorded by Botuverá Cave it is possible to see an additional relationship with mangrove growth and precipitation. This growth was preceded by a peak in depleted values (high precipitation) at Botuverá cave, which points out that onset of mangrove ecosystem was linked to a more southward ITCZ position, more intense SACZ, and wetter conditions in the study area. Observed stem growth in mangrove species has been directly associated to periods of higher precipitation and temperature (Chowdhury et al., 2008; De Alvarenga et al., 2017). Other authors also corroborate the role of precipitation in cambial activity of mangrove species, which in turn affect processes such as stomatal conductance (Robert et al., 2014). Some subtropical mangroves, for example, underwent remarkably increasing in stem radial growth during the wetter season, whose growth was associated to rainfall (Krauss et al., 2006). Thereby, precipitation and temperature play a very important role on dynamics growth of mangrove species.

Moreover, TOC presented higher values than in the previous phase ($\bar{X} = 0.69\%$), while C:N ratio also showed higher values ($\bar{X} = 6.31$). Such increases may be closely tied to mangrove establishment, as it began to produce and preserve more organic matter through *Laguncularia* forests as well as spores, palms, trees-shrubs, which reached their peaks. Accordingly, C₃ plants provided more continental origin to organic matter signal (Fig. 8).

Indeed, RWP is acknowledged as a recent warm period in the northern hemisphere during the late Holocene (Yan et al., 2014; Seppä et al., 2009), commonly related to increased moisture supply in many regions (Haas, 1996; Ji et al., 2005; Seidenkrantz et al., 2007; Martín-Puertas et al., 2009; Wang et al., 2012). Its origin and causes are still not

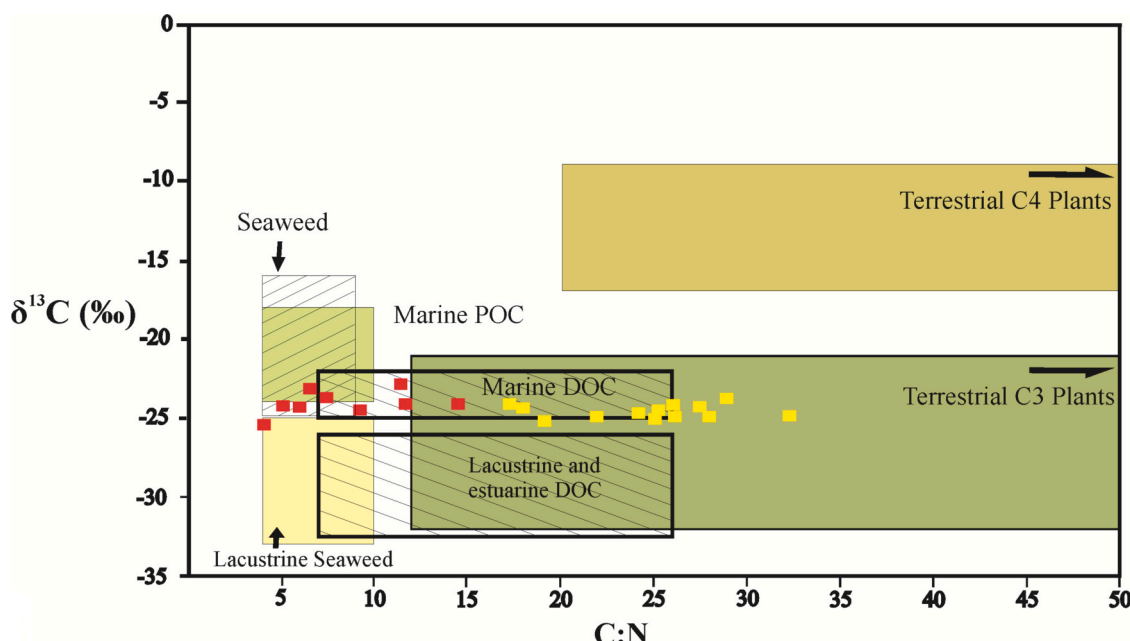


Fig. 8. Binary diagram showing the relationship between $\delta^{13}\text{C}$ and C/N (Meyers, 2003) of intertidal flat (facies association 2, red squares) and supratidal flat facies association (facies association 3, yellow squares) pointing a predominance change on organic matter origin to more continental influence toward top of core SF8. POC = Particulate Organic Carbon, DOC = Dissolved Organic Carbon. (For interpretation of the references to colour in this figure legend, the reader is referred to the web version of this article.)

elucidated (Holmquist et al., 2016). South American studies approaching this epoch are concentrated along south-west side of the continent, while in the southeast they are very sparse (Flantua et al., 2016). Most records show that during RWP this region shifted toward a wetter regime (Behling, 1995, 1997, 2003; Behling et al., 2001; Behling and Safford, 2010; Jeske-Pieruschka and Behling, 2012). Our data agree with this general pattern, moving toward wetter paleoclimatic conditions during RWP.

During much of the DACP, the $\delta^{18}\text{O}$ of Botuverá Cave exhibited depleted values (high precipitation). Nevertheless, our humidity proxies do not reflect this rising rainfall pattern. Overall DACP record involving our SF8 mangrove shows a slight diminish (650 yrs. C.E.). Only at the end of this epoch, when Botuverá record had a marked peak, did SF8 exhibit an abrupt expansion (Fig. 9, dashed black line). Again, our records appear to be only partially sensitive to ITCZ shifts, when major southward movements promoted higher humidity in this region and may have led to mangrove expansion.

The DACP has generally been regarded as a cold period around Europe, the North Atlantic, Arctic regions, North America, the China/Tibetan Plateau, and the northern Pacific (Helama et al., 2017), in turn related to greater North Atlantic ice-rafting, weak North Atlantic Oscillation and/or El Niño–Southern Oscillation (Bond et al., 1997; Berglund, 2003; Reimann et al., 2011; Ügen et al., 2012; Cui and Chang, 2013; Li et al., 2016). Previous studies further indicate a weakening of northern hemisphere monsoon systems due to redistribution of the heat received, giving rise to a southward migration of ITCZ (Braconnot et al., 2007). In southeast South America, this epoch is regarded as a wet paleoclimate (Behling, 1995, 1997, 2003; Behling et al., 2001; Behling and Safford, 2010; Jeske-Pieruschka and Behling, 2012), whereas in southern South America it marks move from wet to dry (Sepúlveda et al., 2009). For the most part, the DACP SF8 palynological signal reflects fewer wet conditions; the paleoclimate became wetter only at the end of this epoch.

Spore content of core SF1 presents a diminishing trend from RWP and the beginning of MCA (Fig. 9a), while its mangrove forest showed an increasing pattern (Fig. 9b), denoting decreasing of moisture supply, but suitable conditions to mangrove establishment.

5.3. FA3 - Supratidal flat facies association (~1100 yrs. C.E. to present)

The upper part of the SF8 site, FA3, was interpreted as a classical supratidal flat environment (upper portion of a progradational tidal flat), due to the presence of massive mud and heterolytic lenticular bedding (Lb) facies superimposed by a mangrove (Daidu et al., 2013). Classic supratidal flats are often covered with vegetation over clay/fine silt substrate showing a higher concentration of organic matter (Daidu et al., 2013). Between ~1000 to ~1600 yrs. C.E. (~MCA to ~LIA) SF8 mangrove exhibited stabilization, expanded again only from ~1700 yrs. C.E.

Depleted values of $\delta^{13}\text{C}$ ($\bar{x} = 24.39\text{\textperthousand}$) indicate more substantial continental influence, coherent with a mangrove expansion and influence of type C₃ vegetation marked by *Rhizophora* (Fig. 8). Colonization by the genus *Rhizophora* was probably fundamental for the increase of primary production in the study area throughout supratidal flat. Hydrological conditions influence the *Rhizophora* species distribution (Numbere and Camilo, 2017), once they are a low salt-tolerant species (Lugo, 1980). They are found at the fringes of the woods in contact with the sea, along channels, at the mouth of some rivers, or in the inner parts of estuaries where salinity is not very high (França et al., 2019). Although they tolerate salinities of up to 55 psu, they grow best when these values around 35 psu or less (Schaeffer-Novelli and Lacerda, 1994). Genus *Rhizophora* is also related to mangroves in advanced stages of development (Soares, 1999; de Souza and Sampaio, 2001; Kilca et al., 2010), to silty substrate (Dornelles et al., 2006), and to air temperature (Duke et al., 1998; Quishoudt et al., 2012; França et al., 2019). In our study area, *Rhizophora* data agree with the findings of some previous researchers (e.g., Duke et al., 1998), namely in that it predominated in silty sand and sandy silt soil composition. *Laguncularia*, however, presented some disparity, being found in both soils with varying grain size (sand, silt, and clay).

Throughout most part of LIA, SF8 mangrove and ferns remained low and stable despite the increasing precipitation trend evidenced by $\delta^{18}\text{O}$ Botuverá Cave data in the beginning of this epoch (Fig. 9c-e). Our data shows that study area vegetation does not respond to this ITCZ southward migration, even though it usually contributes to wetter climate

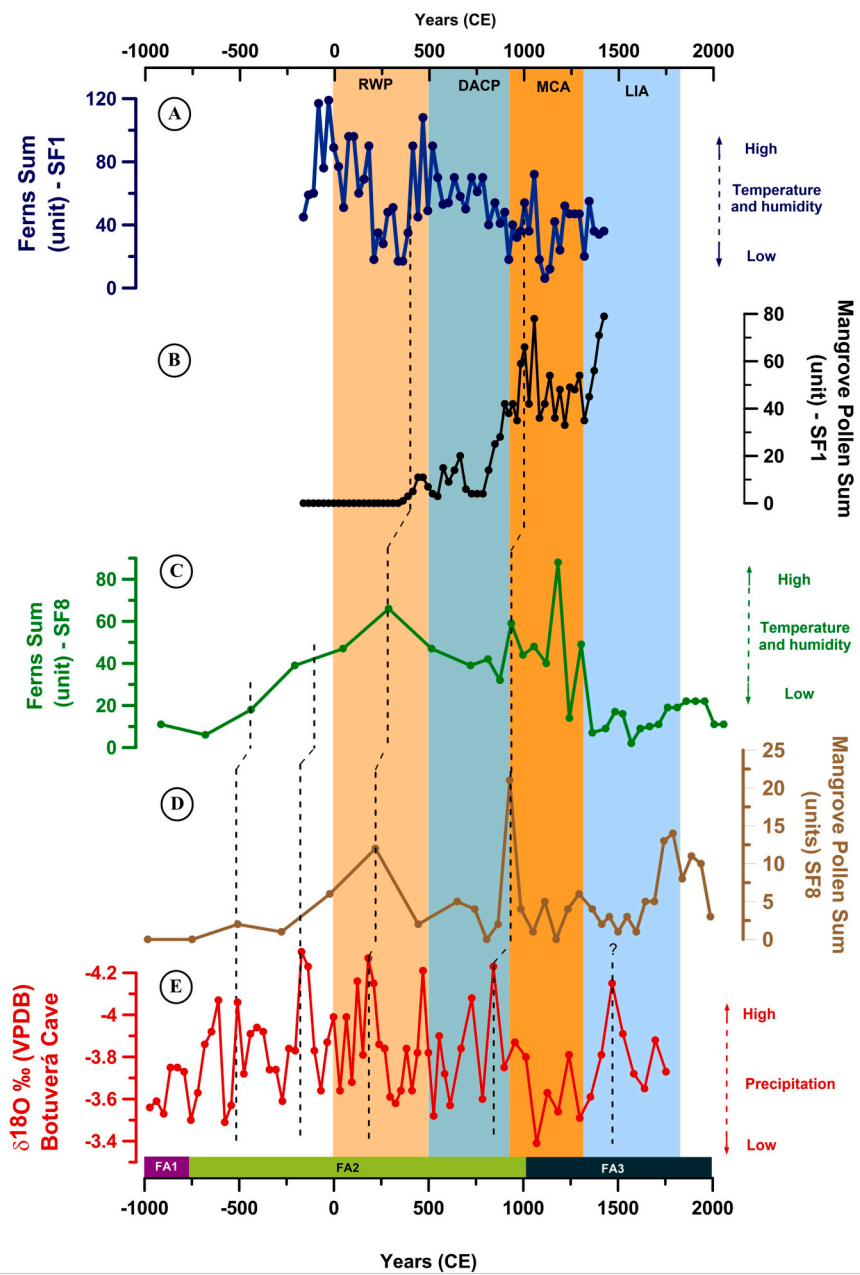


Fig. 9. Integrated sum pollen and isotope data from nearby southernmost mangrove limit in South America. A) Spores content of core SF1 (França et al., 2019) located at northwestern margin of Babitonga Bay, B) Mangrove content of core SF1 (França et al., 2019), C) Spore amount of core SF8 (this study), which was recovered at northeastern margin of Babitonga Bay, D) Mangrove quantity observed throughout core SF8, and E) $\delta^{18}\text{O}$ data from Botuverá Cave records (Bernal et al., 2016), which is ~120 km far from core SF8. Dashed black lines = peaks of precipitation at Botuverá Cave. RWP = Roman Warm Period, DACP = Dark Age Cold Period, MCA = Medieval Climate Anomaly, LIA = Little Ice Age, FA1 = Facies Association 1 (Subtidal Flat), FA2 = Facies Association 2 (Intertidal Flat), FA3 = Facies Association 3 (Supratidal Flat), and C.E. = Common Era.

conditions at other sites in southern South America (Behling, 1995, 1997, 2003; Behling et al., 2001; Behling and Safford, 2010; Jeske-Pieruschka and Behling, 2012) for which reason other environmental factors must force mangrove evolution at our particular study site.

5.4. South Atlantic Subtropical Anticyclone (SASA) and Intertropical Convergence Zone (ITCZ) as rainfall drivers of Babitonga Bay

Precipitation recorded by the $\delta^{18}\text{O}$ of speleothem from Botuverá Cave can be interpreted in the light of ITCZ latitudinal migration during the late Holocene (Bernal et al., 2016), along the lines of other cave studies (Novello et al., 2018). Our pollen, elemental, and isotopic records show a major relation with most depleted values of Botuverá, humid conditions (~ mid RWP, end of DACP); but different patterns also emerge. The difference is especially clear during the LIA, when our spores and mangrove record shows some retraction despite high precipitation at Botuverá Cave (Fig. 9) and surrounding cave locations (e.g., Cristal Cave at southeastern Brazil, Novello et al., 2012, 2018). A likely

explanation is that Babitonga Bay was facing drier and/or colder conditions affecting mangrove development. However, we can discard low temperatures during the LIA in the studied coastal area, as diverse records point toward an increase in sea surface temperature (SST) in the South Atlantic Ocean (Chiessi et al., 2014). For instance, one modern interpretation holds that the recent increase in SST in the South Atlantic Ocean led to the intensification of SASA in 2014, and reduced precipitation in southeast Brazil (Coelho et al., 2016). Therefore, our palynological data probably reflect ITCZ movements, but would also be sensitive to further climate forcings. We put forth that intense/weak SASA could have affected the vegetation (Fig. 10).

During the LIA, enhanced SST in the South Atlantic Ocean (at ~33°S) was connected to a strong Brazil Current as well as weak Atlantic Meridional Overturning Circulation (Chiessi et al., 2014). South Atlantic SST modulates the South Atlantic Subtropical Dipole (SASD), which in turn reflects on SASA and creates a rainfall dipole over South America. Positive phase of SASD is related to warmer waters on its southwestern pole (30°S to 50°S) and colder on its northeastern pole (0° to 30° S). This

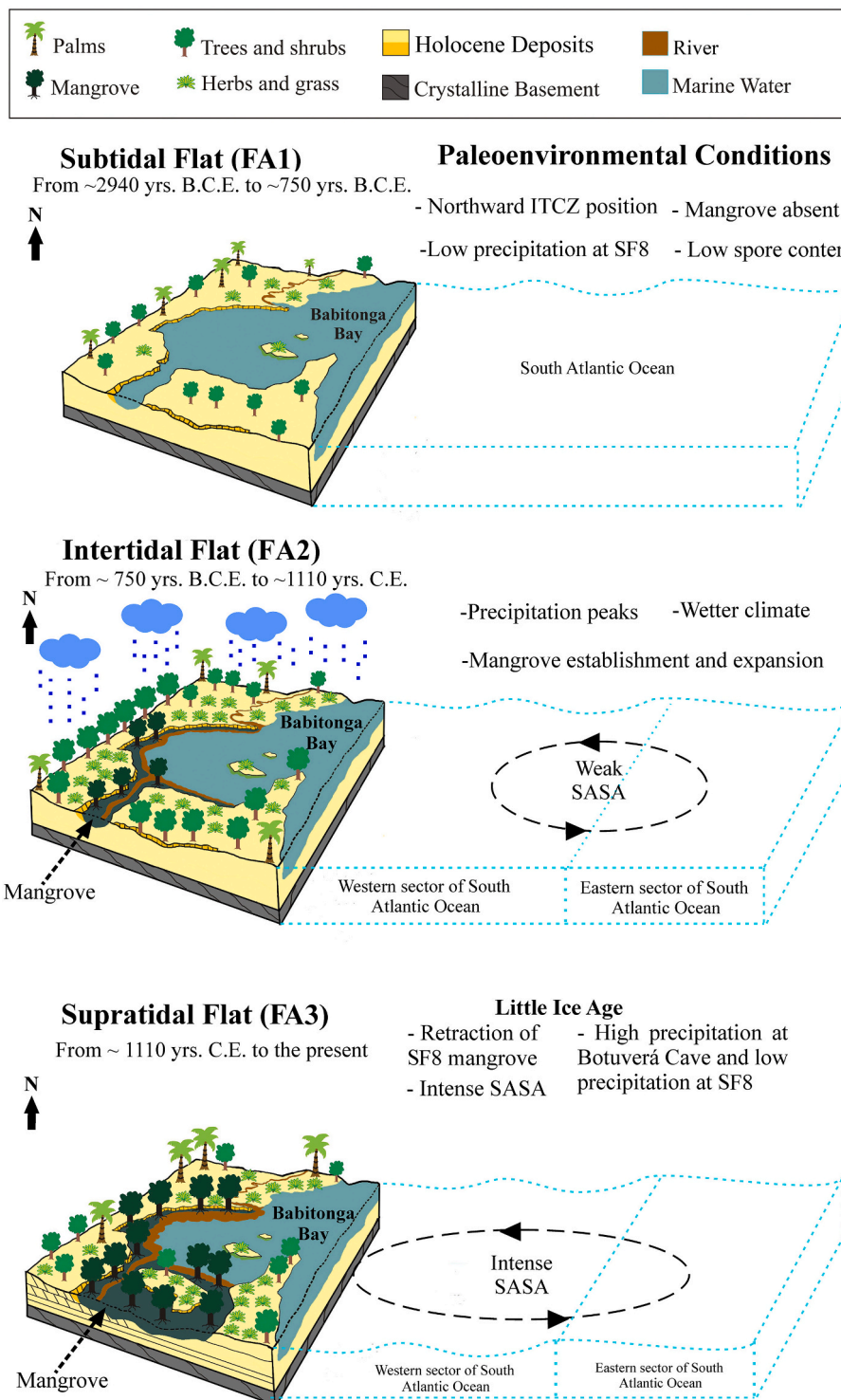


Fig. 10. Paleoenvironmental reconstitution of Babitonga Bay northeastern margin (southern Brazil). From top to the bottom blocks show the evolution of study area. RWP = Roman Warm Period, DACP = Dark Age Cold Period, FA1 = Facies Association 1, FA2 = Facies association 2, FA3 = Facies Association 3, SASA = South Atlantic Subtropical Anticyclone.

pattern is attributed to increased evaporation in the southwestern pole and consequently, decreased moisture advection to northeastern pole through South Atlantic Subtropical Anticyclone resulting in drier conditions to these regions (Wainer et al., 2014). Thereby, air-sea interaction likely created suitable conditions for the development of an intense SASA, influencing the Brazilian southern coastal region through drier conditions. In other words, our palynological data may reflect ITCZ

movements, but would also be sensitive to other climate forcings such as too intense/weak SASA. Our interpretation lies in agreement with studies that point to regional precipitation along Atlantic coastal areas in South America as not only forced by ITCZ migrations, but to sea surface temperatures and trade winds (Utida et al., 2019). Therefore, precipitation is seen to be an essential controlling factor in the appearance and expansion of mangroves during the late Holocene, regulating nutrients,

productivity (Snedaker, 1995), and ultimately mangrove survival (Tomlinson, 1998).

6. Conclusions

Sedimentological data of core SF8 allowed the reconstruction of surrounding Babitonga bay paleoenvironment during the late Holocene. Six facies were identified and grouped into three facies association, from the base to top: subtidal (~2940 yrs. B.C.E. to ~750 yrs. C.E.), intertidal (~750 to ~1100 yrs. C.E.), and supratidal flat (~1100 yrs. C.E. to the present). Elemental and isotopic data reveal a progressive increase in continental influence of organic matter, likely due to the appearance of the mangrove ecosystem (~500 yrs. C.E.) at the studied bay.

A comparison between our palynological data and precipitation patterns reconstructed by $\delta^{18}\text{O}$ Botuverá Cave and other records provide new insights about the influence of the Intertropical Convergence Zone (ITCZ) on hydrological control by near southernmost South America mangroves during the late Holocene. During the Little Ice Age, SF8 mangrove did not respond to the precipitation peak imposed by the most southward ITCZ position, probably due to an intense South Atlantic Subtropical Anticyclone that created drier conditions for the study area. Our interpretation agrees with studies to point that regional precipitation along South America Atlantic coastal areas not only forced by ITCZ migrations, but also to South Atlantic SST dipole. Further studies are needed in order to evaluate the role of hydrological forcing into mangrove forest evolution.

Declaration of Competing Interest

The authors declare that they have no known competing financial interests or personal relationships that could have appeared to influence the work reported in this paper.

Acknowledgments

The authors thank the Coastal Dynamic Laboratory (LADIC-UFPa), C-14 Laboratory of the Center for Nuclear Energy in Agriculture (CENA-USP), University of Joinville (UNIVILLE) and Radiocarbon Laboratory (LAC-UFF) for all infrastructure and support. We also thank three anonymous Reviewers and Prof. H. Falcon-Lang for their constructive comments. The first and third author thanks Brazilian Council for Technology and Science-CNPq for fellowship (process 131813/2016-1, 165911/2015-8 and 305074/2017-2). This study was financed by CNPq (445111/2014-3, 405060/2013-0) and FAPESP (2011/00995-7, 2017/03304-1, and 2020/13715-1). This study also was financed in part by the Coordenação de Aperfeiçoamento de Pessoal Nível Superior – Brazil (CAPES) – Finance Code 001.

References

- Absy, M.L., 1979. A Palynological Study of Holocene Sediments from the Amazon Basin. Ph.D. Thesis. University of Amsterdam (86 p.).
- Absy, M.L., Cleef, A., Fournier, M., Martin, L., Servant, M., Sifeddine, A., Ferreira da Silva, M., Soubies, F., Suguio, K., Turcq, B., Van Der Hammen, T.H., 1991. Mise en Evidence de Quatre Phases D'ouverture de la Forêt Dense dans le Sud-est de l'Amazonie au Cours des 60,000 Dernières Années. Première Comparaison Avec D'autres Régions Tropicales. Comptes Rendus de l'Académie des Sciences, 312, pp. 673–678.
- Anderberg, M.R., 1973. Cluster Analysis for Applications, Probability and Mathematical Statistics: A Series of Monographs and Textbooks. Academic Press, New York (376 p.).
- Angulo, R.J., Lessa, G.G., 1997. The Brazilian sea-level curves: a critical review with emphasis on the curve from Paranaguá and Cananéia regions. Mar. Geol. 140, 161–166. [https://doi.org/10.1016/S0025-3227\(97\)00015-7](https://doi.org/10.1016/S0025-3227(97)00015-7).
- Angulo, R.J., Gianini, P.C.F., Suguio, K., Pessenda, L.C.R., 1999. Relative Sea-level changes in the last 5,500 years in southern Brazil (Laguna Imbituba region, Santa Catarina State) based on vermetid ^{14}C ages. Mar. Geol. 159, 323–339. [https://doi.org/10.1016/S0025-3227\(98\)00204-7](https://doi.org/10.1016/S0025-3227(98)00204-7).
- Baran, E., 1999. A review of quantified relationships between mangroves and coastal resources. Phuket Marine Biol. Center Res. Bull. 62, 57–64.
- Barbier, E.B., 2000. Valuing the environment as input: review of applications to mangrove-fishery linkages. Ecol. Econ. 35, 47–61. [https://doi.org/10.1016/S0921-8009\(00\)00167-1](https://doi.org/10.1016/S0921-8009(00)00167-1).
- Barros, G.V., Martinelli, L.A., Oliveira Novais, T.M., Ometto, J.P.H.B., Zuppi, G.M., 2010. Stable isotopes of bulk organic matter to trace carbon and nitrogen dynamics in an estuarine ecosystem in Babitonga Bay (Santa Catarina, Brazil). Sci. Total Environ. 408, 2226–2232. <https://doi.org/10.1016/j.scitotenv.2010.01.060>.
- Basei, M.A.S., Siga Jr., O., Machiavelli, A., Mancini, F., 1992. Evolução tectônica dos terrenos entre os Cinturões Ribeira e Dom Feliciano (PR-SC). Revista Brasileira de Geociências 22, 216–221. <https://doi.org/10.25249/0375-7536.1992216221>.
- Bauermann, S.G., 2003. Análises palinológicas e evolução paleovegetacional e paleoambiental das turfeiras de Barrocadas e Águas Claras, planície costeira do Rio Grande do Sul, Brasil. In: 137f. Tese (Doutorado). Instituto de Geociências, Curso de Pós-Graduação em Geociências Universidade Federal do Rio Grande do Sul, Porto Alegre.
- Behling, H., 1993. Untersuchungen zur spätpleistozänen und holozänen vegetations und klimgeschichte der tropischen küstenwälder in Santa Catarina (Südbrasiliens). Diss. Botanicae 206, 1–149.
- Behling, H., 1995. A high resolution Holocene pollen record from Lago do Pires, SE Brazil: vegetation, climate and fire history. J. Paleolimnol. 14, 253–268. <https://doi.org/10.1007/BF00624247>.
- Behling, H., 1997. Late quaternary vegetation, climate and fire history of the Araucaria forest and Campos region from Serra Campos Gerais, Paraná State (South Brazil). Rev. Palaeobot. Palynol. 97, 109–121. [https://doi.org/10.1016/S0034-6667\(96\)00065-6](https://doi.org/10.1016/S0034-6667(96)00065-6).
- Behling, H., 2003. Late glacial and Holocene vegetation, climate and fire history inferred from Lagoa Nova in the southeastern Brazilian lowland. Veg. Hist. Archaeobotany 12, 263–270. <https://doi.org/10.1007/s00334-003-0020-9>.
- Behling, H., Safford, H.D., 2010. Late-glacial and Holocene vegetation, climate and fire dynamics in the Serra dos Órgãos, Rio de Janeiro State, southeastern Brazil. Glob. Chang. Biol. 16, 1661–1671. <https://doi.org/10.1111/j.1365-2486.2009.02029.x>.
- Behling, H., Bauermann, S.G., Pereira Neves, P.C., 2001. Holocene environmental changes in the São Francisco de Paula region, southern Brazil. J. S. Am. Earth Sci. 14, 631–639. [https://doi.org/10.1016/S0895-9811\(01\)00040-2](https://doi.org/10.1016/S0895-9811(01)00040-2).
- Berglund, B.E., 2003. Human impact and climate changes - synchronous events and a causal link? Quat. Int. 104, 7–12. [https://doi.org/10.1016/S1040-6182\(02\)00144-1](https://doi.org/10.1016/S1040-6182(02)00144-1).
- Bernal, J.P., Cruz, F.W., Strikis, N.M., Wang, X., Deininger, M., Catunda, M.C.A., Ortega-Obregón Cheng, H., Edwards, R.L., Auler, A.S., 2016. High-resolution Holocene south American monsoon history recorded by a speleothem from Botuverá Cave, Brazil. Earth Planet. Sci. Lett. 450, 186–196. <https://doi.org/10.1016/j.epsl.2016.06.008>.
- Birks, H.J.B., Webb, T., Berti, A.A., 1975. Numerical analysis of pollen samples from central Canada: a comparison of methods. Rev. Palaeobot. Palynol. 20 (3), 133–169.
- Blaauw, M., Christeny, J.A., 2011. Flexible paleoclimate age-depth models using an autoregressive gamma process. Bayesian Anal. 6 (3), 457–474. <https://doi.org/10.1214/11-BA618>.
- Bond, G., Showers, W., Cheseby, M., Lotti, R., Almasi, P., deMenocal, P., Priore, P., Cullen, H., Hajdas, I., Bonani, G., 1997. A pervasive millennial-scale cycle in North Atlantic Holocene and glacial climates. Science 278, 1257–1266. <https://doi.org/10.1126/science.278.5341.1257>.
- Braconnot, P., Otto-Bliesner, B., Harrison, S., Joussaume, S., Pe-terchmitt, J.-Y., Abe-Ouchi, A., Crucifix, M., Driesschaert, E., Fichefet, Th., Hewitt, C.D., Kageyama, M., Kitoh, A., Loutre, M.-F., Marti, O., Merkel, U., Ramstein, G., Valdes, P., Weber, L., Yu, Y., Zhao, Y., 2007. Results of PMIP2 Coupled Simulations of the Mid-Holocene and Last Glacial Maximum – Part 2: Feed-Backs with Emphasis on the Location of the ITCZ and Mid- and High Latitudes Heat Budget. Climate of Past, 3, pp. 279–296. <https://doi.org/10.5194/cp-3-279-2007>.
- Bush, M.B., Miller, M.C., De Oliveira, P.E., Colinvaux, P.A., 2002. Orbital forcing signal in sediments of two Amazonian lakes. Journal of Paleolimnology, In: , 27, pp. 341–352.
- Cannicci, S., Burrows, D., Fratini, S., Smith, T.J., Offenberg, J., Dahdouh-Guebas, F., 2008. Faunistic impact on vegetation structure and ecosystem function in mangrove forests: A review. Aquat. Bot. 89, 186–200. <https://doi.org/10.1016/j.aquabot.2008.01.009>.
- Chiessi, C.M., Mulitza, S., Groeneveld, J., Silva, J.B., Campos, M.C., Gurgel, M.H.C., 2014. Variability of the Brazil Current during the late Holocene. Palaeogeography, Palaeoclimatology, Palaeoecology, 415, 28–36. In: .
- Chowdhury, M.Q., Schmitz, N., Verheyden, A., Sass-Klaassen, U., Koedam, N., Beeckman, H., 2008. Nature and periodicity of growth rings in two Bangladeshi mangrove species. IAWA Journal, In: , 29, pp. 265–276.
- Cintrón-Molero, G., Schaeffer-Novelli, Y., 1992. Ecology and Management of New World Mangroves, Coastal Plant Communities of Latin America. Academic Press, Inc. <https://doi.org/10.1016/B978-0-08-092567-7.50021-0>.
- Coelho, C.A.S., Oliveira, C.P., Ambrizzi, T., Reboita, M.S., Carpenedo, C.B., Campos, J.L. P.S., Tomazziello, A.C.N., Pampuch, L.A., Custódio, M.S., Dutra, L.M.M., da Rocha, R. P., Rehbein, A., 2016. The 2014 Southeast Brazil austral summer drought: regional scale mechanisms and teleconnections. Clim. Dyn. 46, 3737–3752. <https://doi.org/10.1007/s00382-015-2800-1>.
- Cohen, M.C.L., Rodrigues, E., Rocha, D.O.S., Freitas, J., Fontes, N.A., Pessenda, L.C.R., Souza, A.V., Gomes, V.L.P., França, M.C., Bonotto, D.M., Bendassoli, J.A., 2020. Southward migration of the austral limit of mangroves in South America. Catena 195. <https://doi.org/10.1016/j.catena.2020.104775>.
- Colinvaux, P., De Oliveira, P.E., Patiño, J.E.M., 1999. Amazon Pollen Manual and Atlas. British library in publishing data.

- Cui, J., Chang, H., 2013. The possible climate impact on the collapse of an ancient urban city in Mu Us Desert, China. *Reg. Environ. Chang.* 13, 353–364. <https://doi.org/10.1007/s10113-012-0345-y>.
- Daidu, F., Yuan, W., Min, L., 2013. Classifications, sedimentary features and facies associations of tidal flats. *J. Palaeogeogr.* 2, 66–80. <https://doi.org/10.3724/SP.J.1261.2013.00018>.
- Dalrymple, R.W., 1992. Tidal depositional systems. In: Walker, R.G., James, N.P. (Eds.), *Facies Models: Response to Sea Level Change*. Geological Association of Canada, St. John's, pp. 195–218.
- Dalrymple, R.W., 2010. Tidal depositional systems. In: James, N.P., Dalrymple, R.W. (Eds.), *Facies Models 4*. Geological Association of Canada, St. John's, pp. 201–232.
- Dalrymple, R.W., Baker, E.K., Harris, P.T., Hughes, M.G., 2003. Sedimentology and stratigraphy of a tide-dominated, foreland-basin delta (Fly River, Papua New Guinea). *SEPM Spec. Publ.* 76, 147–173. <https://doi.org/10.2110/pec.03.76.0147>.
- De Alvarenga, A.M.S.B., Botosso, P.C., Soffiatti, P., 2017. Stem growth and phenology of three subtropical mangrove tree species. *Brazilian Journal of Botany.*, In: , 40, pp. 907–914, 10.1007/s40415-017-0397-9.
- de Rodrigues, F.O., Lamparelli, C.C., de Moura, D.O., 1999. Environmental impact in mangrove ecosystems: São Paulo, Brazil. In: Yáñez-Arancibia, A., Lara-Domínguez, A.L. (Eds.), *Ecosistemas de Manglar en América Tropical*. Instituto de Ecología A.C. México, IUCN/ORMA, Costa Rica, NOAA/NMFS Silver Spring MD USA, pp. 175–198 (380 p).
- de Souza, M.M.A., Sampaio, E.V.S.B., 2001. Variação temporal da estrutura dos bosques de mangue de Suape-PE após a construção do porto. *Acta Bot. Bras.* 15, 1–12. <https://doi.org/10.1590/S0010-2330620010000100001>.
- DHN - Diretoria de Hidrografia e Navegação Tábua das marés - Porto de São Francisco do Sul/SC, 2017. Banco Nacional de Dados Oceanográficos. Available at: www.mar.mil.br (Accessed in 23/11/2017).
- Donato, D.C., Kauffman, J.B., Murdiyarso, D., Kurnianto, S., Stidham, M., Kanninen, M., 2011. Mangroves among the most carbon-rich forests in the tropics. *Nat. Geosci.* 4, 293–297. <https://doi.org/10.1038/NGEO1123>.
- Dornelles, S.S., Moreira, G.M., Freitas, L.M., 2006. Caracterização da estrutura dos manguezais do canal do Linguaço, baía da Babitonga. In: Cremer, M.J., et al. (Eds.), *(Org.) Diagnóstico ambiental da baía da Babitonga*. Joinville: Univille, pp. 187–199.
- Duke, N.C., Ball, M.C., Ellison, J.C., 1998. Factors influencing biodiversity and distributional gradients in mangroves. *Glob. Ecol. Biogeogr. Lett.* 7, 27–47. <https://doi.org/10.2307/2997695>.
- Ellison, A.M., 2002. Macroecology of mangroves: Large-scale patterns and processes in tropical coastal forests. *Trees Struct. Funct.* 16, 181–194. <https://doi.org/10.1007/s00468-001-0133-7>.
- Faegri, K., 1966. Some problems of representativity in pollen analysis. *Palaeobotanist*. In: , 15, pp. 135–140.
- Fan, D.D., 2011. Open-coast tidal flats. In: Davis Jr., R.A., Dalrymple, R.W. (Eds.), *Principles of Tidal Sedimentology*. Springer, New York, pp. 187–229. <https://doi.org/10.3724/SP.J.1261.2013.00018>.
- FEMAR - Fundação de Estudos do Mar, 2000. *Catálogo de Estações Maregráficas Brasileiras*, Rio de Janeiro.
- Plantua, S.G.A., Hooghiemstra, H., Vuille, M., Behling, H., Carson, J.F., Gosling, W.D., Hoyos, I., Ledru, M.P., Montoya, E., Mayle, F., Maldonado, A., Rull, V., Tonello, M.S., Whitney, B.S., González-Aragón, C., 2016. Climate variability and human impact in South America during the last 2000 years: synthesis and perspectives from pollen records. *Clim. Past* 12, 483–523. <https://doi.org/10.5194/cp-12-483-2016>.
- França, M.C., Pessenda, L.C., Cohen, M.C., de Azevedo, A.Q., Fontes, N.A., Silva, F.B., Macario, K., 2019. Late-Holocene subtropical mangrove dynamics in response to climate change during the last millennium. *The Holocene* 29, 445–456. <https://doi.org/10.1177/0959683618816438>.
- FUNDEMA, 1994. Fundação Municipal de Meio Ambiente. *Programa de Proteção da Biodiversidade e dos Recursos Hídricos da Região de Joinville*, SC. Centro de Desenvolvimento Biotecnológico, 56p. .
- Garreaud, R.D., Vuille, M., Compagnucci, R., Marengo, J., 2009. Present-day south American climate. *Palaeogeogr. Palaeoclimatol. Palaeoecol.* 281, 180–195. <https://doi.org/10.1016/j.palaeo.2007.10.032>.
- Gonçalves, M.L., Kaul, P.F.T., 2002. Evolução Geológica. In: kNIE, J. L. W.(Org.) (Ed.), *Atlas Ambiental da Região de Joinville: Complexo Hídrico da Baía da Babitonga*. Florianópolis: FATMA/GTZ, 1 ed., pp. 05–08.
- Gonçalves, M.L., Zanotelli, C.T., Oliveira, F.A., 2006. Diagnóstico e Prognósticas Disponibilidades e Demandas Hídricas do Rio Cubatão do Norte – Joinville – Santa Catarina. *Editora da Univille*, Joinville (96p).
- González, C., Urrego, L.E., Martínez, J.I., 2006. Late Quaternary vegetation and climate change in the Panama Basin: Palynological evidence from marine cores ODP 677B and TR 163–38. *Palaeogeogr. Palaeoclimatol. Palaeoecol.* 234, 62–80. <https://doi.org/10.1016/j.palaeo.2005.10.019>.
- Gordon, A.D., 1981. Classification Methods for the Exploratory Analysis of Multivariate Data. Chapman and Hall, London (193 p).
- Grimm, E.C., 1987. CONISS: a FORTRAN 77 program for stratigraphically constrained cluster analysis by the method of incremental sum of squares. *Comput. Geosci.* 13, 13–35.
- Grimm, E.C., 1990. TILIA and TILIAGRAPH: PC spreadsheet and graphic software for pollen data. In: INQUA Sub-Commission on Data-Handling Methods Newsletter, 4, pp. 5–7.
- Haarsma, R.J., Campos, J.D.E., Hazeleger, W., Severijns, C., Piola, A.R., Molteni, F., 2005. Dominant modes of variability in the South Atlantic: A study with a hierarchy of ocean-atmosphere models. *J. Clim.* 18, 1719–1735. <https://doi.org/10.1175/JCLI3370.1>.
- Haas, J.N., 1996. Pollen and plant macrofossil evidence of vegetation change at Wallisellen-Langachermoos (Switzerland) during the Mesolithic–Neolithic transition 8,500 to 6,500 years ago. *Diss. Botanicae* 267, 1–67.
- Hamilton, S.E., Casey, D., 2016. Creation of a high spatio-temporal resolution global database of continuous mangrove forest cover for the 21st century (CGMFC-21). *Glob. Ecol. Biogeogr.* 25, 729–738. <https://doi.org/10.1111/geb.12449>.
- Helama, S., Jones, P.D., Briffa, K.R., 2017. Dark Ages Cold Period: A literature review and directions for future research. *The Holocene* 27, 1600–1606. <https://doi.org/10.1177/0959683617693898>.
- Herz, R., 1991. *Manguezais do Brasil - 1988*. Instituto Oceanográfico da USP/ Cimr, São Paulo (233 p).
- Hogg, A.G., Heaton, T.J., Hua, Q., Palmer, J.G., Turney, C.S.M., Southon, J., Bayliss, A., Blackwell, C., Boswijk, G., Bronk Ramsey, C., Pearson, C., Petchey, F., Reimer, P., Reimer, R., Wacker, L., 2020. SHCal20 Southern Hemisphere calibration, 0–55,000 years cal BP. *Radiocarbon* 62. <https://doi.org/10.1017/RDC.2020.59>.
- Holmquist, J.R., Booth, R.K., MacDonald, G.M., 2016. Boreal peatland water table depth and carbon accumulation during the Holocene thermal maximum, Roman warm period and medieval climate Anomaly. *Palaeogeogr. Palaeoclimatol. Palaeoecol.* 444, 15–27. <https://doi.org/10.1016/j.palaeo.2015.11.035>.
- Hooghiemstra, H., Van der Hammen, T., 1998. Neogene and Quaternary development of the neotropical rain forest: the forest refugia hypothesis, and a literature overview. *Earth Sci. Rev.* 44, 147–183 (doi: 10.1016/S0012-8252(98)00027-0).
- IBGE - Instituto Brasileiro de Geografia e Estatística, 2004. *Mapa de Biomas e Vegetação do Brasil*.
- IPCC, 2013. In: Stocker, T.F., Qin, D., Plattner, G.-K., Tignor, M., Allen, S.K., Boschung, J., Midgley, P.M. (Eds.), *Climate Change 2013: The physical science basis. Contribution of working group I to the fifth assessment report of the intergovernmental panel on climate change*. Cambridge University Press, Cambridge, United Kingdom and New York, NY, USA. <https://doi.org/10.1017/CBO9781107415324>, 1535 pp.
- Jeske-Pieruschka, V., Behling, H., 2012. Palaeoenvironmental history of the São Francisco de Paula region in southern Brazil during the late Quaternary inferred from the Rincão das Cabritas core. *The Holocene* 22, 1251–1262. <https://doi.org/10.1177/0959683611414930>.
- Ji, J., Shen, J., Balsam, W., Chen, J., Liu, L., Liu, X., 2005. Asian monsoon oscillations in the northeastern Qinghai–Tibet Plateau since the late glacial as interpreted from visible reflectance of Qinghai Lake sediments. *Earth Planet. Sci. Lett.* 233, 61–70.
- Jones, M.C., Wingard, G.L., Stackhouse, B., Keller, K., Willard, D., Marot, M., Landacre, B., E., and Bernhardt, C., 2019. Rapid inundation of southern Florida coastline despite low relative sea-level rise rates during the late-Holocene. *Nat. Commun.* 10, 3231. <https://doi.org/10.1038/s41467-019-11138-4>.
- Kathiiresan, K., Bingham, B.L., 2001. Biology of mangroves and mangrove ecosystems. *Adv. Mar. Biol.* 40, 81–251. [https://doi.org/10.1016/S0065-2881\(01\)40003-4](https://doi.org/10.1016/S0065-2881(01)40003-4).
- Kilca, R.V., do Costa, M.P., Zanini, R.R., Carvalho, F.A., da Costa, A.F., 2010. Estrutura de manguezais em diferentes estágios sucessionais no estuário do rio Piauí, Sergipe-Brasil. *Pesquisas Botânicas* 61, 171–189.
- Kodama, Y., 1992. Large-scale common features of subtropical precipitation zones (the Baiu Frontal Zone, the SP CZ, and the SACZ) part I: Characteristics of Subtropical Frontal zones. *J. Meteorol. Soc. Jpn.* 70, 813–836.
- Krauss, K.W., Doyle, T.W., Twilley, R.R., Rivera-Monroy, V.H., Sullivan, J.K., 2006. Evaluating the relative contributions of hydroperiod and soil fertility on growth of south Florida mangroves. *Hydrobiologia.*, In: , 569, pp. 311–324.
- Krauss, K.W., McKee, K.L., Lovelock, C.E., Cahoon, D.R., Saintilan, N., Reef, R., Chen, L., 2014. How mangrove forests adjust to rising sea level. *New Phytol.* 202, 19–34. <https://doi.org/10.1111/nph.12605>.
- Lessa, G., Angulo, R.J., Giannini, P.C.F., Araújo, A.D., 2000. Stratigraphy and Holocene evolution of a regressive barrier in south Brasil. *Mar. Geol.* 165, 87–108. [https://doi.org/10.1016/S0025-3227\(99\)00130-9](https://doi.org/10.1016/S0025-3227(99)00130-9).
- Li, C., Han, C., Wang, P., 1992. Depositional sequences and storm deposition on low-energy coast of China. *Acta Sedimentol. Sin.* 10 (4), 119–127.
- Li, G., Dong, H., Hou, W., Wang, S., Jiang, H., Yang, J., Wu, G., 2016. Temporal succession of ancient phytoplankton community in Qinghai Lake and Implication for Paleoenvironmental change. *Sci. Rep.* 6, 1–12. <https://doi.org/10.1038/srep19769>.
- Liebmann, B., Mechoso, C., 2011. The South American Monsoon system. In: Chang, C.P., et al. (Eds.), *The Global Monsoon System: Research and Forecast*, 2nd ed. World Scientific Publication Company, p. 608.
- Lugo, A.E., 1980. Mangrove ecosystems: successional or steady state? *Biotropica* 12, 65–72.
- Marengo, J.A., Liebmann, B., Grimm, A.M., Misra, V., Silva Dias, P.L., Cavalcanti, I.F.A., Carvalho, L.M.V., Berbery, E.H., Ambrizzi, T., Vera, C.S., Saulo, A.C., Nogues-Paegle, J., Zipser, E., Seth, A., Alves, L.M., 2012. Recent developments on the South American monsoon system. *Int. J. Climatol.* 32, 1–21. <https://doi.org/10.1002/joc.2254>.
- Martin, L., Dominguez, J.M.L., Bittencourt, A.C.S.P., 2003. Fluctuating Holocene Sea levels is eastern and southeastern Brazil: evidence from a multiple fossil and geometric indicators. *J. Coast. Res.* 19, 101–124.
- Martín-Puertas, C., Valero-Garcés, B.L., Brauer, A., Mata, M.P., Delgado-Huertas, A., Dulski, P., 2009. The Iberian–Roman Humid Period (2600–1600 cal yr BP) in the Zoñar Lake varve record (Andalucía, southern Spain). *Quat. Res.* 71, 108–120. <https://doi.org/10.1016/j.yqres.2008.10.004>.
- Mazzer, A.M., Gonçalves, M.L., 2012. Aspectos geomorfológicos da Baía da Babitonga. Caracterização Morfométrica. *Revista Brasileira de Geomorfologia*, Santa Catarina, Brasil, p. 12. <https://doi.org/10.20502/rbg.v1i20.264>.
- McIvor, A., Möller, I., Spencer, T., 2012a. Reduction of Wind and Swell Waves by Mangroves Cambridge Coastal Research Unit Working Paper 40. Nat. Coast. Protect. Ser. 1–27.

- McIvor, A., Spencer, T., Möller, I., 2012b. Storm surge reduction by mangroves. In: Natural Coastal Protection Series: Report, 2.
- McIvor, A., Spencer, T., Möller, I., Spalding, M., 2016. World Bank - Managing Coasts with Natural Solutions: Guidelines for Measuring and Valuing the Coastal Protection Services of Mangroves and Coral Reefs, pp. 24–53.
- McKee, K.L., 2011. Biophysical controls on accretion and elevation change in Caribbean mangrove ecosystems. *Estuar. Coast. Shelf Sci.* 91, 475–483. <https://doi.org/10.1016/j.ecss.2010.05.001>.
- McKee, K., Rogers, K., Saintilan, N., 2012. Response of salt marsh and mangrove wetlands to changes in atmospheric CO₂, climate and sea level. In: Global Change and the Function and Distribution of Wetlands, pp. 63–96. <https://doi.org/10.1007/978-94-007-4494-3>.
- Menéndez, P., Losada, I.J., Torres-Ortega, S., Narayan, S., Beck, M.W., 2020. The global flood protection benefits of mangroves. *Sci. Rep.* 10, 1–11. <https://doi.org/10.1038/s41598-020-61136-6>.
- Menghini, R.P., 2004. Dinâmica da regeneração natural de bosques de mangue impactados na Ilha Barnabé, Baixada Santista, São Paulo, Brasil. In: 125f. Tese (Doutorado em Oceanografia Biológica) - Universidade de São Paulo, São Paulo.
- Meyers, P.A., 1994. Preservation of elemental and isotopic source identification of sedimentary organic matter. *Chem. Geol.* 114, 289–302. [https://doi.org/10.1016/0099-2541\(94\)90059-0](https://doi.org/10.1016/0099-2541(94)90059-0).
- Meyers, P.A., 2003. Applications of organic geochemistry to paleolimnological reconstructions: a summary of examples from the Laurentian Great Lakes. *Org. Geochem.* 34, 261–289.
- Moreno, A., Pérez, A., Frigola, J., Nieto-Moreno, V., Rodrigo-Gámiz, M., Martrat, B., González-Samperiz, P., Morellón, M., Martín-Puertas, C., Corella, J.P., Belmonte, Á., Sancho, C., Cacho, I., Herrera, G., Canals, M., Grimalt, J.O., Jiménez-Espejo, F., Martínez-Ruiz, F., Vegas-Villarrubia, T., Valero-Garcés, B.L., 2012. The medieval climate Anomaly in the Iberian Peninsula reconstructed from marine and lake records. *Quat. Sci. Rev.* 43, 16–32. <https://doi.org/10.1016/j.quascirev.2012.04.007>.
- Morioka, Y., Tozuka, T., Yamagata, T., 2011. On the growth and decay of the Subtropical Dipole mode in the South Atlantic. *J. Clim.* 24, 5538–5554. <https://doi.org/10.1175/2011jcli4010.1>.
- Munsell Color, 2009. Munsell Soil Color Charts. New Revised Edition. Macbeth Division of Kollmorgen Instruments, New Windsor, NY.
- Nagelkerken, I., Blaber, S.J.M., Bouillon, S., Green, P., Haywood, M., Kirton, L.G., Meynecke, J.-O., Pawlik, J., Penrose, H.M., Sasekumar, A., Somerfield, P.J., 2008. The habitat function of mangroves for terrestrial and marine fauna: A review. *Aquat. Bot.* 89, 155–185. <https://doi.org/10.1016/j.aquabot.2007.12.007>.
- Neukom, R., Steiger, N., Gómez-Navarro, J.J., Wang, J., Werner, J.P., 2019. No evidence for globally coherent warm and cold periods over the preindustrial Common Era. *Nature* 571, 550–554. <https://doi.org/10.1038/s41586-019-1401-2>.
- Neves, P.C.P. das, Bach, F., Rossoni, M.G., Bauermann, S.G., Kroeff, V.N., Augustin, R., Prochnow, E.A., 2001. Novas ocorrências de pôlen de Magnoliophyta no Quaternário do Estado do Rio Grande do Sul. *Pesquisas – Série Botânica*, In: , 51, ., pp. 59–71
- Nnamchi, H.C., Li, J., Anyadike, R.N.C., 2011. Does a dipole mode really exist in the South Atlantic Ocean? *J. Geophys. Res.* 116, D15104. <https://doi.org/10.1029/2010JD015579>.
- Novello, V.F., Cruz, F.W., Karmann, I., Burns, S.J., Strikis, N.M., Vuille, M., Cheng, H., Edwards, R.L., Santos, R.V., Frigo, E., Barreto, E.A.S., 2012. Multidecadal climate variability in Brazil's Northeast during the last 3000 years based on speleothem isotope records. *Geophys. Res. Lett.* 39, L23706. <https://doi.org/10.1029/2012GL053936>.
- Novello, V.F., Cruz, F.W., Moquet, J.S., Vuille, M., de Paula, M.S., Nunes, D., Edwards, R. L., Cheng, H., Karmann, I., Utida, G., Strikis, N.M., Campos, J.L.P.S., 2018. Two millennia of South Atlantic Convergence Zone variability reconstructed from isotopic proxies. *Geophys. Res. Lett.* 45, 5045–5051. <https://doi.org/10.1029/2017GL076838>.
- Numbere, A.O., Camilo, G.R., 2017. Effect of temperature and precipitation on global mangrove Rhizophora species distribution. *Am. J. Environ. Sci.* 13, 342–350. <https://doi.org/10.3844/ajessp.2017.342.350>.
- Orloci, L., 1967. An agglomerative method for classification of plant communities. *J. Ecol.* 55 (1), 193–206.
- Pessenda, L.C.R., Gouveia, S.E.M., Aravenab, R., Boulet, R., Valencia, E.P.E., 2004. Holocene fire and vegetation changes in southeastern Brazil as deduced from fossil charcoal and soil carbon isotopes. *Quat. Int.* 114, 35–43. [https://doi.org/10.1016/S1040-6182\(03\)00040-5](https://doi.org/10.1016/S1040-6182(03)00040-5).
- Pielou, E.C., 1984. *The Interpretation of Ecological Data: A Primer on Classification and Ordination*. John Wiley & Sons, New York (288 p).
- Quisthoudt, K., Schmitz, N., Randin, C.F., Dahdouh-Guebas, F., Robert, E.M.R., Koedam, N., 2012. Temperature variation among mangrove latitudinal range limits worldwide. *Trees - Struct. Funct.* 26, 1919–1931. <https://doi.org/10.1007/s00468-012-0760-1>.
- Reimann, T., Tsukamoto, S., Harff, J., Osadczuk, K., Frechen, M., 2011. Reconstruction of Holocene coastal foredune progradation using luminescence dating – an example from the Świnia barrier (southern Baltic Sea, NW Poland). *Geomorphology* 132, 1–16. <https://doi.org/10.1016/j.geomorph.2011.04.017>.
- Reineck, H.E., Singh, I.B., 1980. *Depositional Sedimentary Environments* (2nd Edition). Springer-Verlag, Berlin, p. 549.
- Robert, E.M.R., Jambia, A.H., Schmitz, N., De Ryck, D.J.R., De Mey, J., Kairo, J.G., Dahdouh-Guebas, F., Beeckman, H., Koedam, N., 2014. How to catch the patch? A dendrometer study of the radial increment through successive cambia in the mangrove Avicennia. *Annals of Botany*, In: , 113, pp. 741–752, 10.1093/aob/mcu001.
- Rosa, R.O., 2002. Geomorfologia. W. (Org.). In: Knie, J.L. (Ed.), *Atlas Ambiental de Joinville*. Fatma/GTZ.
- Roubik, D.W., Moreno, J.E., 1991. Pollen and Spores of Barro Colorado Island. Missouri Botanical Garden. Monographs in Systematic Botany, 36 (268 p).
- Schaeffer-Novelli, Y., Lacerda, L.D., 1994. Manguezais. In: *Diagnosticos Ambiental Oceanico e Costeiro das Regiões sul e Sudeste do Brasil*. Fundesp/Iousp/Petrobras, São Paulo.
- Schaeffer-Novelli, Y., Cintrón-Molero, G., Adame, R.R., de Camargo, T.M., 1990. Variability of mangrove ecosystems along the Brazilian coast. *Estuaries* 13, 204–218. <https://doi.org/10.2307/1351590>.
- Schaeffer-Novelli, Y., Cintrón-Molero, G., Soares, M.L.G., De-Rosa, T., 2000. Brazilian mangroves. *Aquat. Ecosyst. Health Manag.* 3, 561–570. <https://doi.org/10.1080/1463498008650693>.
- Schaeffer-Novelli, Y., Soriano-Sierra, E.J., Do Vale, C.C., Bernini, E., Rovai, A.S., Pinheiro, M.A.A., Schmidt, A.J., De Almeida, R., Coelho Júnior, C., Menghini, R.P., Martinez, D., de Abuchahla, G.M.O., Cunha-Lignon, M., Charlher-Sarubo, S., Shirazava-Freitas, J., Cintrón-Molero, G., 2016. Climate changes in mangrove forests and salt marshes. *Braz. J. Oceanogr.* 64, 37–52. <https://doi.org/10.1590/S1679-875920160919064sp2>.
- Schwamborn, R., Saint-Paul, U., 1996. Mangroves – forgotten forests? *Nat. Resour. Dev.* 43 (44), 13–36.
- Seidenkrantz, M.S., Aagaard-Sørensen, S., Sulsbrück, H., Kuipers, A., Jensen, K.G., Kunzendorf, H., 2007. Hydrography and climate of the last 4,400 years in a SW Greenland fjord: implication for Labrador Sea palaeoceanography. *The Holocene* 17, 387–401 (doi: 10.1177/0959683607075840).
- Seppä, H., Bjune, A.E., Telford, R.J., Birks, H.J.B., Veski, S., 2009. Last nine-thousand years of temperature variability in Northern Europe. *Clim. Past* 5, 523–535. <https://doi.org/10.5194/cp-5-523-2009>.
- Septulveda, J., Pantoja, S., Hughen, K.A., Bertrand, S., Figueiroa, D., León, T., Drenzek, N. J., Lange, C., 2009. Late Holocene sea-surface temperature and precipitation variability in northern Patagonia, Chile (Jacaf Fjord, 44°S). *Quaternary Research*, 72, 400–409. In: , 10.1016/j.yqres.2009.06.010.
- Snedaker, S.C., 1995. Mangroves and climate change in Florida and Caribbean region: scenarios and hypotheses. In: *Proceedings of the Asia-Pacific Symposium on Mangrove Ecosystems*. Springer, Netherlands, pp. 43–49. https://doi.org/10.1007/978-94-011-0289-6_6.
- Soares, M.L.G., 1999. Estrutura vegetal e grau de perturbação dos manguezais da Lagoa da Tijuca, Rio de Janeiro, RJ, Brasil. *Rev. Bras. Biol.* 59, 503–515. <https://doi.org/10.1590/s0034-7108199900300016>.
- Spalding, M., Kainuma, M., Collins, L., 2010. *World atlas of mangroves*. A collaborative project of ITTO, ISME, FAO, UNEP-WCMC, UNESCO-MAB, UNU-INWEH and TNC. London (UK): Earthscan, London (319 pp).
- Stockmarr, J., 1971. Tablets with spores used in absolute pollen analysis. *Pollen Spores* 13, 615–621.
- Stramma, L., England, M., 1999. On the water masses and mean circulation of South Atlantic Ocean. *J. Geophys. Res.* 104, 20,863–20,883. <https://doi.org/10.1029/1999JC00139>.
- Stuiver, M., Reimer, P.J., Reimer, R.W., 2021. CALIB 8.2 [WWW program]. <http://calib.org>. (Accessed 1 April 2021).
- Thampanya, U., Vermaat, J.E., Sinsakul, S., Panapitukkul, N., 2006. Coastal erosion and mangrove progradation of Southern Thailand. *Estuar. Coast. Shelf Sci.* 68, 75–85. <https://doi.org/10.1016/j.ecss.2006.01.011>.
- Tomazelli, L.J., Villwock, J.A., 2000. O Cenozoico no Rio Grande do Sul: geologia da planície costeira. In: Holz, M., De Ros, L.F. (Eds.), *Geologia do Rio Grande do Sul*. Edição CIGO/UFRGS, Porto Alegre, pp. 375–406.
- Tomlinson, P.B., 1998. *Rhizophora* in Australasia-some clarification of taxonomy and distribution. *J. Arnold Arbor. 79*, 156–169.
- Ülgen, U.B., Franz, S.O., Biltekin, D., Çagatay, M.N., Roeser, P.A., Doner, L., Thein, J., 2012. Climatic and environmental evolution of Lake İznik (NW Turkey) over the last ~4,700 years. *Quat. Int.* 274, 88–101. <https://doi.org/10.1016/j.quaint.2012.06.016>.
- Utida, G., Cruz, F.W., Etourneau, J., Bouloubassi, I., Schefuß, E., Vuille, M., Novello, V.F., Prado, L.F., Sifeddine, A., Klein, V., Zular, A., Viana, J.C.C., Turcq, B., 2019. Tropical South Atlantic influence on Northeastern Brazil precipitation and ITCZ displacement during the past 2300 years. *Sci. Rep.* 9, 1698. <https://doi.org/10.1038/s41598-018-38003-6>.
- Van der Hammen, T., Absy, M.L., 1994. Amazonia during the last glacial. *Palaeogeogr. Palaeoclimatol. Palaeoecol.* 109, 247–261. [https://doi.org/10.1016/0031-0182\(94\)90178-3](https://doi.org/10.1016/0031-0182(94)90178-3).
- Venegas, S.A., Mysak, L.A., Straub, D.N., 1997. Atmosphere–Ocean coupled Variability in the South Atlantic. *J. Clim.* 10, 2904–2920. [https://doi.org/10.1175/1520-0442\(1997\)010<2904:AOCVT>2.0.CO;2](https://doi.org/10.1175/1520-0442(1997)010<2904:AOCVT>2.0.CO;2).
- Vieira, C.V., Horn Filho, N.O., 2007. Carta sedimentológica do complexo estuarino da baía da Babitonga, Santa Catarina, Brasil (CDROM). In: XII Congresso Latinoamericano de Ciências do Mar, 2007, Florianópolis. Anais do XII COLACMAR - Resumos Expandidos CDROM, 30052, pp. 1–3.
- Viero, A.C., Silva, D.R.A., 2016. Geodiversidade do Estado de Santa Catarina. Porto Alegre, CPRM. Programa Geologia do Brasil - PGB. Levantamento da Geodiversidade, available in: <http://rigeo.cprm.gov.br/jspui/handle/doc/14712>.
- Villwock, J.A., Tomazelli, L.J., Loss, E.L., Dehnhardt, E.A., Horn, N.O., Bach, F.A., Dehnhardt, B.A., 1986. Geology of the Rio Grande do Sul coastal province. In: Rabassa, J. (Ed.), *Quaternary of South America and Antarctic Peninsula*. A. A. Balkema, Rotterdam, 4, pp. 79–97.
- Vuille, M., Burns, S.J., Taylor, B.L., Cruz, F.W., Bird, B.W., Abbott, M.B., Kanner, L.C., Cheng, H., Novello, V.F., 2012. A review of the south American monsoon history as

- recorded in stable isotopic proxies over the past two millennia. *Clim. Past* 8, 1309–1321. <https://doi.org/10.5194/cp-8-1309-2012>.
- Wainer, I., Prado, L.F., Khodri, M., Otto-Bliesner, B., 2014. Reconstruction of the South Atlantic Subtropical Dipole index for the past 12,000 years from surface temperature proxy. *Sci. Rep.* 4, 5291. <https://doi.org/10.1038/srep05291>.
- Walker, R.G., James, N.P., 1992. Facies models and modern stratigraphic concepts. In: Walker, R.G., James, N.P. (Eds.), *Facies Models - Response to Sea Level Change*. Geological Association of Canada, Ontario, Canada, pp. 1–14.
- Wang, T., Surge, D., Mithen, S., 2012. Seasonal temperature variability of the Neoglacial (3300 – 2500 BP) and Roman warm period (2500–1600 BP) reconstructed from oxygen isotope ratios of limpet shells (*Patella vulgata*), Northwest Scotland. *Palaeogeogr. Palaeoclimatol. Palaeoecol.* 317–318, 104–113. <https://doi.org/10.1016/j.palaeo.2011.12.016>.
- Ward, J.H., 1963. Hierarchical grouping to optimize an objective function. *J. Am. Stat. Assoc.* 58 (301), 236–244.
- Wentworth, C.K., 1922. Clastic sediments. *J. Geol.* 30, 377–392. <https://doi.org/10.1086/622910>.
- Yan, H., Sun, L., Shao, D., Wang, Y., Wei, G., 2014. Higher sea surface temperature in the northern South China Sea during the natural warm periods of late Holocene than recent decades. *Chin. Sci. Bull.* 59, 4115–4122. <https://doi.org/10.1007/s11434-014-0317-3>.
- Zhou, J., Lau, K.M., 1998. Does a monsoon climate exist over South America? *J. Clim.* 11, 1020–1040. [https://doi.org/10.1175/1520-0442\(1998\)011<1020:DAMCEO>2.0.CO;2](https://doi.org/10.1175/1520-0442(1998)011<1020:DAMCEO>2.0.CO;2).